AGU PUBLICATIONS

JGR

Journal of Geophysical Research: Atmospheres

RESEARCH ARTICLE
10.1002/2017JD028004

Key Points:
- Probable enhancement of rainfall at urban and downwind regions relative to the rainfall upwind of major cities in Northern India is found
- Enhancement of downwind rainfall is influenced by both the urbanized area of the city and ambient aerosol loading during the storm
- Synergy between Urban heat island effect and aerosol microphysical effect results in increase of urban and downwind rainfall around cities

Correspondence to:
S. N. Tripathi,
snt@iitk.ac.in

Citation:
Sarangi, C., Tripathi, S. N., Qian, Y., Kumar, S., & Ruby Leung, L. (2018). Aerosol and urban land use effect on rainfall around cities in Indo-Gangetic Basin from observations and cloud resolving model simulations. *Journal of Geophysical Research: Atmospheres*, *123*, 3645–3667. https://doi.org/10.1002/2017JD028004

Received 2 NOV 2017
Accepted 27 FEB 2018
Accepted article online 5 MAR 2018
Published online 12 APR 2018

Aerosol and Urban Land Use Effect on Rainfall Around Cities in Indo-Gangetic Basin From Observations and Cloud Resolving Model Simulations

Chandan Sarangi[1,2], S. N. Tripathi[1,3], Yun Qian[2], Shailendra Kumar[3], and L. Ruby Leung[2]

[1]Department of CIVIL Engineering, Indian Institute of Technology, Kanpur, India, [2]Atmospheric Sciences and Global Change Division, Pacific Northwest National Laboratory, Richland, WA, USA, [3]Centre for Environmental Science and Engineering, Indian Institute of Technology, Kanpur, India

Abstract Coupling of urban land use land cover (LULC) and aerosol loading on rainfall around cities in the Gangetic Basin (GB) is examined here. Long-term observations illustrate more rainfall at urban core and climatological downwind regions compared to the upwind regions of Kanpur, a metropolitan area located in central GB. In addition, analysis of a 15 day cloud resolving simulation using the Weather Research and Forecasting model also illustrated similar rainfall pattern around other major cities in the GB. Interestingly, the enhancement of downwind rainfall was greater than that over urban regions, and it was positively associated with both the urban area of the city and ambient aerosol loading during the propagating storm. Further, to gain a process-level understanding, a typical storm that propagated northwestward across Kanpur was simulated using Weather Research and Forecasting under three different scenarios. Case 1 has realistic LULC representation of Kanpur, while the grids representing the Kanpur urban region were replaced by cropland LULC pattern in Case 2. Comparison illustrated that urban heat island effect caused convergence of winds and moisture in the lower troposphere, which enhances convection over urban region and induced more rainfall over the urban core compared to upwind regions. Case 3 is similar to Case 1 but lower aerosol concentration (by a factor of 100) over the storm region. Analysis shows that aerosol-induced microphysical changes delay the initiation of warm rain (over the upwind region) but enhance ice phase particle formation in latter stages (over the urban and downwind regions) resulting in increase in downwind rainfall.

1. Introduction

Land use and land cover (LULC) changes from a rural to an urban land cover can perturb the surface energy fluxes, micrometeorology, convection initiation, cloud dynamics, and surface rainfall (Lowry, 1977; Pielke et al., 2011; Pielke, 2001; Shepherd, 2005). Urbanization-induced changes in surface properties increase surface and near-surface temperature (commonly known as urban heat island effect; UHI, e.g., X. Yang et al., 2017) but reduce moisture availability (Clark et al., 1985; Oke, 2002). UHI effect can destabilize the planetary boundary layer (PBL) and trigger convection by creation of a convergence zone (Bornstein & Lin, 2000; Hand & Shepherd, 2009; Huff & Changnon Jr, 1972; Jauregui & Romales, 1996; Molders & Olson, 2004; Shepherd et al., 2002; B. Yang et al., 2012) that modifies rainfall around cities. However, in propagating storms, the maximum changes in precipitation may occur downwind rather than at the city, and they can vary with different geographical and meteorological backgrounds. In some cases of propagating storms, the spatial heterogeneity in LULC at the juxtaposition of rural lands and urban lands can create a significant contrast in land-atmosphere interactions, bifurcate rainfall systems, delay storm propagation, and reduce urban rainfall (Changnon Jr et al., 1976; Diem & Brown, 2003; Guo et al., 2006; Niyogi et al., 2011). Additionally, lower moisture availability, deeper PBL, and changes in surface hydrology can reduce convective available potential energy (CAPE) and thereby rainfall in urban region (Kaufmann et al., 2007; Zhang et al., 2009). Lastly, the sign of urban effect on rainfall may vary with rain rates (W. Li et al., 2011), synoptic conditions (Yan et al., 2016), and the size and canopy architecture of a city (Schmid & Niyogi, 2013). Overall, urbanization can have a significant effect on regional water availability as well as can cause flash flood hazards (L. Yang et al., 2015), but our understanding of the net association between a city and the occurrence of rainfall around it from propagating storms is still uncertain.

Concurrently, urban locations are associated with increased population and emission of anthropogenic aerosols, which interact with clouds and radiation and influence regional rainfall (Collier, 2006; Orville et al., 2001; Rosenfeld & Woodley, 2003; Zhong et al., 2015, 2017). While some studies showed that increase in aerosol number concentration can cause a decrease in precipitation amounts (Teller & Levin, 2006), other studies indicated more precipitation induced by aerosols because of feedbacks from changes in cloud microphysics and storm dynamics (Khain & Lynn, 2009; Koren et al., 2012; Rosenfeld et al., 2008; Van den Heever et al., 2006). Summarizing a large number of studies, aerosols induced impact on surface rainfall can either be positive or negative (even by more than 100%), depending on environmental conditions, wind shear, aerosols, and cloud types (Fan et al., 2009; Khain et al., 2008; Levin & Cotton, 2008; Z. Li et al., 2016; Qian et al., 2009; Tao et al., 2012). In contrast, using a long-term simulation, Seifert et al. (2012) reported that clouds may themselves act as natural buffers in large-scale cloud systems, resulting in insignificant aerosol-induced changes in overall surface precipitation. Recent studies have focused on the combined effect of aerosols and urban LULC changes on rainfall, but the net impact and the underlying mechanisms are still unclear (Givati & Rosenfeld, 2004; Jin & Shepherd, 2005; Ntelekos et al., 2008; Rosenfeld, 2000; Van den Heever et al., 2006). Molders and Olson (2004) showed modification of the cloud microphysical paths under combined aerosol and UHI effect (see also Van den Heever et al., 2006, and Ntelekos et al., 2008). Therefore, urbanization may also influence precipitation through associated enhancement in aerosol concentration (Zhong et al., 2017). Also, variation in the sign of urban effect on rainfall (in previous studies as discussed above) may be linked to the background aerosol loading over a city during different storms, suggesting that UHI-rainfall relationship may change regionally, both, qualitatively and quantitatively.

The Gangetic Basin (GB) in North India is the most populated river basin in the world and is home to ~700 million people whose livelihood is directly or indirectly linked to the summer monsoonal rainfall. Indian summer monsoon is characterized by mesoscale convective cloud systems which feature mostly mixed phase clouds. Also, the frequency of occurrence of cumulonimbus towers is very high over the GB (Bhat & Kumar, 2015). Generally, rainfall over a city in the GB occurs from propagating storms associated with mesoscale convective systems. These mesoscale systems are typically associated with Indian monsoon lows, which are characterized by cyclonic wind circulation over the Indian landmass and northwest propagation of the relative vorticity of the rain storms after initiation (Boos et al., 2015). Figure 1b marked the locations of many big Indian cities. Rapid industrialization, an emerging economy, and population growth in the last two decades have resulted in high growth rate of urbanization as well as pollution in India, mainly in the GB (Bhagat, 2011; Dey & Di Girolamo, 2011). A recent observational study by Mitra et al. (2012) showed that urbanization in the last 50 years has led to a tenfold increase in rainfall over Kolkata, a large metropolitan located in the eastern GB. In addition, Kishtawal et al. (2010) and Singh et al. (2016) reported the observational signatures of urban-induced rainfall anomaly during the Indian summer monsoon. Using numerical simulations, Lei et al. (2008) showed that localized convection and heavy rainfall over Mumbai, a large metropolitan in western India, may be due to convergence associated with urban circulation. Similar positive associations between urban land use and rainfall have also been reported over Chennai (Simpson et al., 2008). Although a distinct positive effect of urban LULC is emerging from these studies over India, our understanding of the rainfall spatial distribution around Indian cities during propagating mesoscale storms and the physical mechanism, especially over the heavily polluted GB, is still unknown.

On the contrary, Shastri et al. (2015) showed that the UHI effect on rainfall over the GB is negligible compared to the influence of prevalent synoptic scale forcing during summer monsoon. Moreover, the impact of urban aerosols was not considered in the above studies. Recent studies have illustrated that the microphysical impacts of aerosols acting as cloud condensation nuclei (CCN) are significant during the Indian summer monsoon due to a close coupling between cloud dynamics and cloud microphysics. For example, more cloud water can be transported upward due to CCN-induced initial suppression of warm rainfall and increase the freezing of cloud drops to ice phase. The increased releases of latent heat in a polluted environment invigorate the cloud systems to generate more ice hydrometeors and eventually more rain but at a later stage and probably at a downwind location compared to clean conditions (Hazra et al., 2017, 2013; Prabha et al., 2012; Sarangi et al., 2015, 2017). Recent years have witnessed devastating flash floods over various major cities of North India during the monsoon season, causing loss of properties and human life (Gupta & Nair, 2011; http://www.independent.co.uk/news/world/asia/india-floodsbangladesh-nepal-deaths-millions-homeless-latest-news-updates-a7919006.html). Thus, a better understanding of the effect of urbanization and

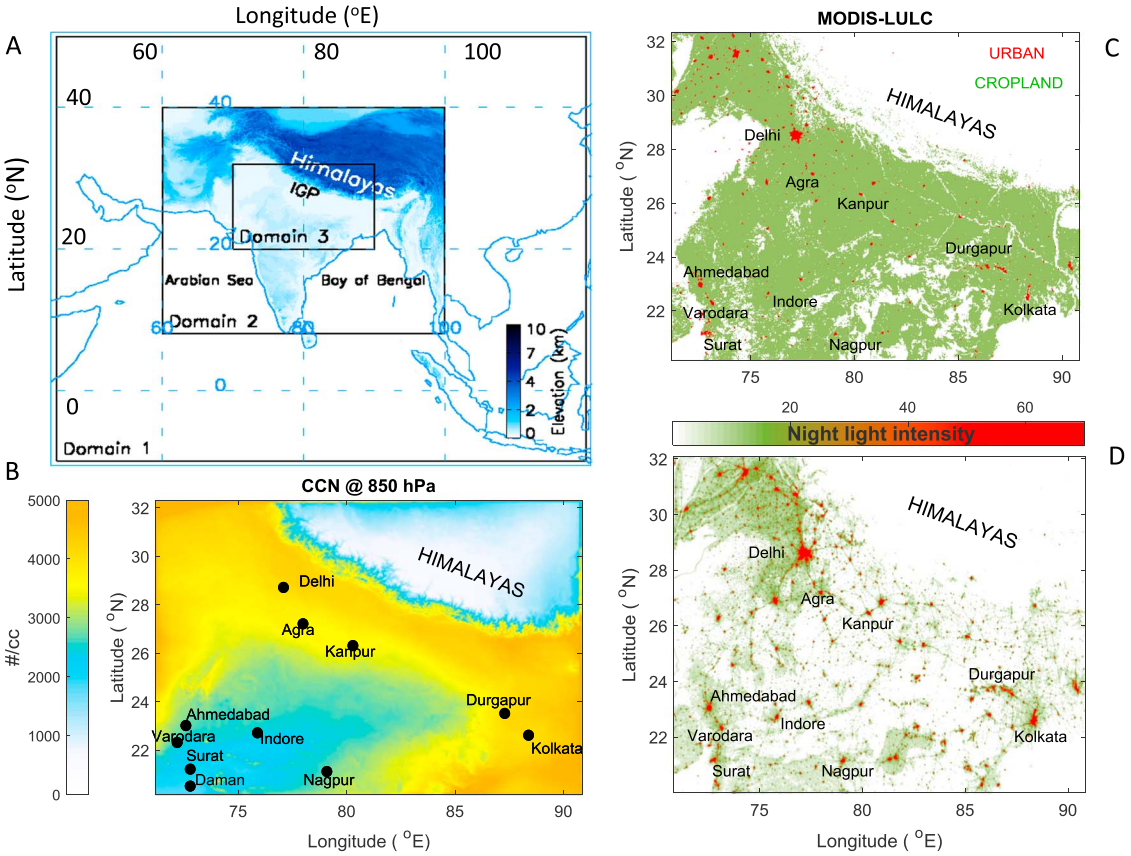

Figure 1. Panel a illustrates an overview map of the nested domains used in all the Weather Research and Forecasting simulations from 5 to 20 August 2011. Shade represents the terrain height. Panels b and c illustrate the mean cloud condensation nuclei (CCN) number concentration simulated and the static LULC representation within Domain 3 of WRF simulations, respectively. The red spots indicate urban grids amidst croplands (green). Panel d shows corresponding mean composite of version 4 cloud-free composites of DMSP-OLS observed nightlight intensity data over Domain 3. Darker light intensity represent more urbanized surface. The data are available at https://ngdc.noaa.gov/eog/dmsp/downloadV4composites.html.

aerosol loading on the magnitude and spatial distribution of summer monsoon rainfall is essential for improving short-term rainfall prediction, water management, and disaster mitigation policies.

In this context, the main objective of this study is to examine the variation in total rainfall over urban regions compared to the nearby rural regions in the GB. Specifically, we investigate whether there is a distinct urban effect on rainfall over the downwind region compared to the upwind region during typical propagating storms across the cities in GB. A recent study over Kanpur, a typical metropolitan located in central GB, used automatic weather station (AWS) network around Kanpur to show very high UHI values, both at surface and at canopy level during the monsoon season (Chakraborty et al., 2016). We use ground-based rainfall measurements from the same network and long-term satellite observations to illustrate an urban signature on rainfall over the greater Kanpur region. The second objective of our study is to examine whether the urban-rainfall associations observed over this representative GB city are also present over different cities located in GB and are consistent for different storm events. An additional question is whether the urban-rainfall relationship over other North Indian cities (with lower ambient pollution) located outside of the GB is different from or similar to that observed over Kanpur. The lack of high-density rain gauge networks within and around cities in North India limits the scope of an observational analysis of these objectives. So we perform a high-resolution simulation of a typical heavy rainfall period from 5 to 20 August 2011 using the Weather Research and Forecasting (WRF) model with the Thompson aerosol-aware microphysics to address our second and third objectives. The simulated rainfall period was associated with mesoscale systems over northern India and contributed to about half of the annual rainfall over this region within a short span of 15 days. Hourly output of simulated rainfall at 3 km spatial resolution provided many samples of propagating

storms across prominent big cities of GB and North India. Details of the data set used, the model setup, model evaluation, and numerical experiments are described in section 2 followed by results and discussions in section 3. The work is summarized in section 4.

2. Data Set and Model Details

2.1. Observations of Rainfall Around Greater Kanpur

Four years (2013–2016) of high-resolution (half-hourly) in situ rainfall measurements are available from a network of three AWSs over the greater Kanpur (shown in Figure 5a). One of the three stations is located at the high-intensity urban center of Kanpur city, while the other two are located at a low-intensity urban site in the northern part of Kanpur city and at a rural site ~10 km south of Kanpur city, respectively. Frequency-intensity comparison of rainfall measured at these sites is performed to establish the difference in frequency and magnitude of rainfall among the urban and rural sites within the network at various time scales. Only measurements between June and September for days when all three sites were operational are included in this analysis. However, this analysis only provides us with comparison between rural regions to the south of Kanpur and the urban regions in Kanpur city.

Further, attenuation-corrected radar reflectivity factor (Z_e) observations from the precipitation radar on board the Tropical Rainfall Measuring Mission (TRMM-PR 2A25, version-7) satellite are used to gain a better overview of the spatial distribution of rainfall over the greater Kanpur region (Iguchi et al., 2000). TRMM is a non-Sun synchronous satellite containing 49 beams, each separated by 0.71° to provide a total swath width of 247 km. It samples the area between 38°S and 38°N several times a day (Kummerow et al., 1998, 2000). TRMM-PR works in the Ku band (13.8 GHz) and has a wavelength of 2.2 cm. Horizontal and vertical resolutions of TRMM-PR are 4.3 km (5 km since August 2001) and 0.25 km, respectively. The TRMM-PR provides a Z_e at 80 vertical levels in dBZ units (dBZ = 10 × $\log_{10}$ Z), where Z is expressed in mm^6m^3. The high spatial resolution is important for determining the climatology and spatial variations of rainfall over the small area. Measurements during the Indian monsoon period, that is, June through September, between 1998 and 2015 are used. We regridded the raw Z_e values into rectangular latitude-longitude grids of 0.05° × 0.05°. In this study, we use Z_e values $>$ 30 dBZ measured at 2 km altitude in each grid box and the climatological mean is calculated to indicate the spatial distribution of rainfall under rainfall events around the greater Kanpur. Lower Z_e values from TRMM-PR has high uncertainty (W. Li & Schumacher, 2011). Moreover, Z_e values $<$30 dBZ at 2 km altitude correspond to rain rate of $<$1 mm/h and may be associated with no surface rainfall (Ulbrich & Atlas, 1998).

2.2. WRF Simulation Setup, Evaluation, and Methodology Used for Analysis

Chang et al. (2009) showed that WRF has good ability in simulating the Indian monsoon depressions. The WRF Model, version 3.6.1, is configured to simulate the regional weather prevalent over India using three nested domains (Figure 1a) during 4–20 August 2011. The outermost domain has a resolution of 27 km and comprises the Southeast Asian region. The innermost domain has a resolution of 3 km, centering over the GB. The intermediate resolution domain (9 km resolution) bridges the resolution difference between the outermost and innermost domains. There are 34 layers between the surface and 50 hPa. The initial and lateral boundary conditions for the meteorological fields are obtained from the NCEP FNL (Final) Operational Global Analysis data available at a resolution of 1° × 1° for every 6 h. A spin-up time of 1 day is used.

The vertical subgrid scale fluxes due to eddy transport in the PBL are parametrized by the Mellor-Yamada-Janjic boundary layer scheme (Janjic, 2002). The Noah land surface model is used to represent land surface processes and the surface energy balance (F. Chen & Dudhia, 2001). The Grell-Freitas cumulus scheme (Grell & Freitas, 2014) is used in the outer and middle domains but the innermost domain explicitly resolves convection at 3 km resolution. The updated two-moment Thompson bulk microphysics scheme is used, which considers five separate species: cloud water, cloud ice, rain, snow, and a hybrid graupel with hail category (Thompson et al., 2008). It also incorporates the activation of water friendly aerosols (proxy for CCN) and ice nuclei (IN), so it explicitly predicts the droplet number concentration of cloud water as well as the number concentrations of CCN and IN. A fraction of the CCN concentration is activated into cloud droplets using a lookup table that determines the fraction as a function of the model-predicted temperature, vertical velocity, CCN concentration, and hygroscopicity parameter and aerosol mean radius (0.04 mm). Upon nucleation, the

participating aerosols are removed from the population, though they can be returned to CCN on evaporation of cloud or rain drops. Wet scavenging is also considered in these simulations. The number of IN particles that nucleate into ice crystals is determined following DeMott et al. (2010) for cases above water saturation to account for condensation and immersion freezing and by following Phillips et al. (2008) in cases that are unsaturated with respect to water saturated to account for deposition nucleation. In addition, the freezing of deliquesced aerosols using the hygroscopic CCN concentration is determined from Koop et al. (2000). Further detailed descriptions of the numerous process rate terms for cloud species, droplet number concentration, CCN, and IN can be found in Thompson et al. (2004, 2008) and Thompson and Eidhammer (2014).

Horizontal and vertical advection of winds, temperature, water vapor, cloud particles, trace gases, IN, and CCN particles are determined using a positive definite, monotonic scheme (H. Wang et al., 2009). CCN and IN number concentrations are mixed consistently with heat, moisture, and momentum fluxes produced by the boundary layer parametrization. The CCN aerosol category is designed as a combination of sulfates, sea salts, and organic matter, while the IN aerosol category mainly resembles dust concentration. Multiyear (2001–2007) global model simulations (Colarco et al., 2010) are performed with prescribed aerosols emitted by natural and anthropogenic sources. Multiple size bins for multiple species of aerosols are simulated by the Goddard Chemistry Aerosol Radiation and Transport model (Ginoux et al., 2001) and used to obtain the mass mixing ratios of sulfates, sea salts, dust, and organic carbon at a 0.58° longitude by 1.25° latitude grid spacing. While the mean dust mass with diameter larger than 0.5 mm is considered IN concentration, a combination of all other species except for black carbon is used as a proxy for the CCN concentration. A method described in Chin et al. (2002) is used to convert the input mass mixing ratio data to number concentrations by assuming lognormal distributions with characteristic diameters and geometric standard deviations. Further details about the global climatology of the aerosol species and the CCN input data are given in Thompson and Eidhammer (2014).

The spatial distribution of mean-simulated CCN values (5–20 August 2011) prevalent at 850 hPa over Domain 3 is shown in Figure 1b. The simulated CCN concentration is $>$2,500 particles per cm^3 over the entire GB. In addition, most of the CCN burden is concentrated within the boundary layer (not shown). It can also be seen that the CCN concentration near the west coast is 2–3 times lower than the GB. Recent surface and aircraft measurements reported similar high CCN concentration (2,000–6,000/cm^3) within the boundary layer during monsoon season over the GB (Bhattu & Tripathi, 2015; Dumka et al., 2015; Roy et al., 2017; Sarangi et al., 2015; Srivastava et al., 2013). Moreover, satellite observations and global modeling studies indicated similar spatial differences in aerosol loading over North India during monsoon season (Misra et al., 2016, and references therein). Thus, this methodology of prescribing CCN emission fluxes as surface source in each grid box and allowing them to physically move around with the meteorological forcing is able to mimic reasonably well the spatial and vertical distribution of CCN over North India. The simulated CCN concentration is used to predict cloud water droplet concentration spectrum in the microphysical module. Further, interactions between clouds and radiation are implemented by linking the predicted cloud water with a constant effective radius from the microphysics scheme with the rapid radiative transfer model for general circulation model radiation scheme (Mlawer et al., 1997).

The 30 min Moderate-Resolution Imaging Spectroradiometer (MODIS) data set provides static geographical fields, such as terrain height, soil properties, vegetation fraction, land use, and albedo, which are interpolated to the domain grids by using the WRF preprocessing system. The LULC of any grid in the model setup is the most dominant LULC type in that area as documented in the MODIS data set. As the model resolution increases, more accurate LULC representation is used in the model. Figure 1c illustrates the LULC defined in each grid of Domain 3 from our simulation. The version 4 cloud-free composites of DMSP-OLS observed nightlight intensity data are also plotted for Domain 3 during August 2011 in Figure 1d to visualize the urbanization scenario. The nightlight data are available at 30 arc sec resolution from https://ngdc.noaa.gov/eog/dmsp/downloadV4composites.html. The high-density urban cities and conglomerates in the GB are evident from the nighttime intensity data set. The entire stretch of the Indo-Gangetic Plains (north part of the GB) from the Himalayan foothills above Delhi to Kolkata near Bay of Bengal is covered by sprawling urban cities. Comparison between Figures 1c and 1d illustrates that Domain 3 with spatial resolution of 3 km is able to well represent the heterogeneity in regional LULC, especially the urban cities over the GB in our model simulations.

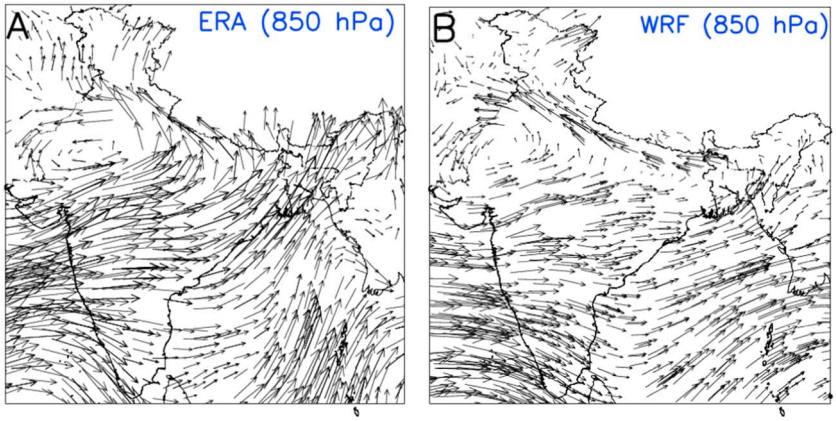

Figure 2. Mean midday (0600 UTC) wind circulation from (a) ERA reanalysis at 850 hpa and (b) Weather Research and Forecasting (WRF)-Domain 2 simulation. Leftward arrow represents 10 ms^{-1}.

2.3. Model Evaluation: Wind Circulation, Rainfall, and Near-Surface Temperature

Using the Domain 2 results, Figure 2 compares the WRF-simulated mean midday wind circulation pattern (5–20 August 2011) with the corresponding wind data from ERA-Interim reanalysis data at 850 hPa. Cyclonic wind circulation is observed over northern India during this period. Over South India the winds blew from Arabian Sea in the west toward Bay of Bengal in the east. The ERA observed wind circulation patterns, their centers, and overall wind speeds are well captured by the model. This wind pattern is consistent with the active phase of Indian monsoon system, which are associated with low-level moisture influx, synoptic

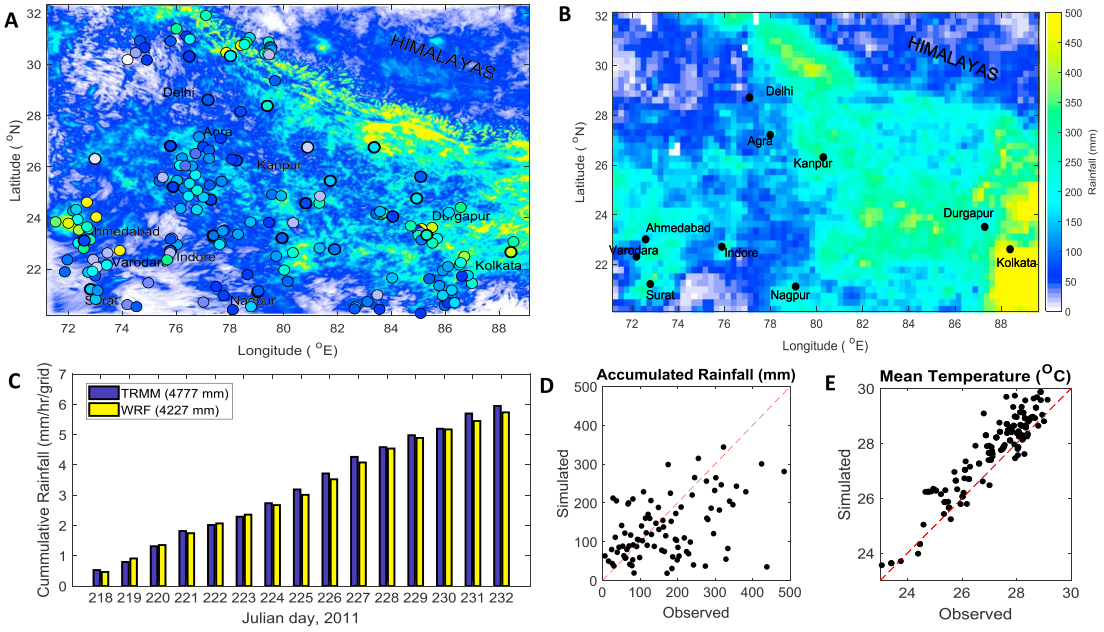

Figure 3. Spatial distribution of accumulated rainfall from (a) Weather Research and Forecasting (WRF)-Domain 3 simulation and (b) Tropical Rainfall Measuring Mission (TRMM)-gridded data set between 5 and 20 August 2011. The colored circles in Panel a are accumulated rainfall observed at in situ measurement sites maintained by Indian Space Research Organization and Global Historical Climatology Network. Panel c compares the time series of cumulative domain total rainfall simulated within Domain 3 of WRF (yellow) with corresponding TRMM measurements (blue) between 5 and 20 August 2011 (Julian day 218–232). Comparison of accumulated rainfall and 2 m temperature between the in situ measurements over Indian Space Research Organization and Global Historical Climatology Network sites and corresponding WRF grids within Domain 3 is shown in Panels d and e, respectively. The observed data set is arranged in an ascending order of accumulated rainfall and divided into 100 bins of 1 percentile each. The observed and corresponding WRF-simulated values are averaged to create 100 scatter points. These scatter points are plotted in Panels d and e.

scale mesoscale cloud systems, and heavy rainfall over central and North India (Krishnamurti & Bhalme, 1976; Sikka, 1977). However, on an average, lower wind speeds are simulated over Indo-Gangetic plains and near the Himalayan foothills compared to reanalysis. These differences may contribute to the biases in simulated rainfall near Himalayan foothills (discussed below).

Figures 3a and 3b compare the spatial distributions of accumulated rainfall amount simulated by WRF and observed by TRMM satellite during 5–20 August 2011 in Domain 3. In general, the GB region received more rainfall (~150 mm in most of the grids) compared to the western part of North India (Figure 3b). Previous studies have reported that during the prevalence of cyclonic wind motion over India, the southeastern regions receive comparatively more rainfall (Krishnamurti & Bhalme, 1976; Sikka, 1977). Comparison with the corresponding WRF-simulated total rainfall distribution illustrates that the model is also able to reproduce the spatial distribution of rainfall over this region reasonably well, but the model values are lower compared to observed values in the middle GB region (Figures 3a and 3b) during this period.

Further, to check if the temporal variation in mesoscale meteorology is well captured by our simulations, we compared the cumulative rainfall amount over Domain 3 with TRMM observations (Figure 3c). The temporal pattern of rainfall occurrence from TRMM and WRF matches well over Domain 3. Cumulative rainfall initially increased steadily between 5 and 10 August 2011. This is followed by steep increase in rainfall from 11 to 15 August 2011. Thereafter, again the increase is gradual till 20 August 2011. The domain total daily rainfall amount from TRMM estimates is also higher compared to the corresponding simulated values in most days. It should be noted that TRMM retrievals are over a coarser grid and are calculated by assuming the same rain rate over an interval of 3 h, so the TRMM estimates might also have inherent uncertainties.

As an additional check, we used ground-based in situ measurements within Domain 3 to evaluate our model-simulated rainfall amount. Most of the rain gauge station data used in our evaluation are part of the AWS network maintained by Indian Space Research Organization, and the data are available at http://www.mosdac.gov.in/. We also used measurements from stations that are part of the Global Historical Climatology Network (GHCN) and are located within Domain 3. The GHCN-daily data are available at https://www.ncdc.noaa.gov/. The accumulated rainfall during 5–20 August 2011 is calculated from measurements at each station and plotted as scatter points corresponding to its location on the latitude-longitude axes in Figure 3a. In total data from 192 sites (all sites where data are available from both Indian Space Research Organization and GHCN networks within our study region and period) are used. The scatter points are colored with the same scale used to represent accumulated WRF rainfall in Figure 3a. Comparison of the scatter points against the background contour shows that WRF was able to reasonably simulate the heterogeneity in spatial pattern of accumulated rainfall at local scales. For example, spatial variations seen in accumulated rainfall from the site measurements near the Himalayan foothills (increase as we move northeastward from 30°N;74°E toward 32°N;80°E), in the GB (increase as we move northeastward from 20°N;83°E toward 24°N;88°E.), central India (first increase and then decrease as we move northeastward from 21°N;79°E toward 23°N;83°E), and the western part of North India (increases as we move northwestward from 21°N;73°E toward 24°N;72°E) are well captured by our convection permitting WRF simulation. However, similar to the TRMM comparison, negative biases are present in the simulated magnitudes compared to in situ observations especially over the northern parts of the GB region near the Himalayan foothills. This may be partly related to the observed biases in simulated wind circulation (Figure 2). Further, good correlation (correlation coefficient = 0.6 at 95% confidence interval) between the in situ measured accumulated rainfall values and simulated accumulated rainfall over corresponding WRF grid in Domain 3 is seen (Figure 3d). However, the good correlation was mostly due to the stations over the plain regions of North India. We found that correlation coefficient of the association (similar to Figure 3d) is lower ($<$0.3) for the stations in Himalayan foothills. In addition, similar evaluation of simulated rainfall at daily and subdaily scale shows that the model was not able to accurately simulate the exact time and location of rainfall event (generally, the correlation coefficient was $<$0.2 over most of the stations in Himalayan foothills) even at 3 km resolution. Figure 3e illustrates the comparison between temporal mean 2 m temperatures observed at these AWS stations and Domain 3 simulated 2 m temperature values during our study period. The sample points lie very close to the 1:1 line indicating good skills of WRF (correlation coefficient = 0.9 at 95% confidence interval) to simulate the near-surface temperature. However, for stations with higher background temperature values (mainly north of the GB in our case), we found that the simulated values were slightly higher than observed values, largely due to negative biases in accumulated rainfall as seen in Figure 3d.

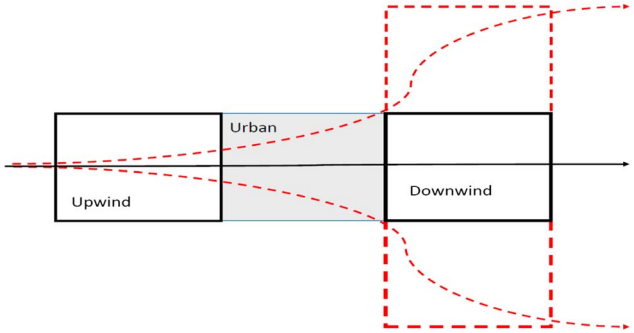

Figure 4. Schematic drawn for ease of visualizing the upwind, downwind, and urban region during the propagating storm events. In case the direction of storm propagation is west to east over a typical city (center gray-shaded box) in North India (as shown by black arrow), the upwind box is considered as an area equal to the urban region but located to the west of the gray box. Similarly, the downwind box is considered as an area equal to the urban region but to the east of the gray box. In our analysis, we have considered eight such major directions of storm propagation corresponding to the storm entering the urban region from the eight quadrants of a circle. However, the storms may follow three pathways of exit as shown here by arrows. In such cases the downwind region is considered as the region shown in red boxes.

The resolution difference in the observations (~25 km and point measurement) and model simulation (3 km) might be the reason behind the bias in rainfall magnitude and mean temperature. Besides, these biases may also be attributed to the coarse data input and uncertainties associated with the physical parametrizations of temperature, pressure, winds, and moisture during our simulation period. As the model was not nudged with data assimilation, the error propagation in prognostic variables may increase with time and space, which can also contribute to the biases seen in our simulations. Moreover, satellite retrievals over mountainous regions have high uncertainty which can also limit the accurate representation of rainfall in observations. Nevertheless, these simulations are able to well capture the spatial and daily variations in mesoscale meteorology as well as the LULC heterogeneity, and the 3-D distribution of CCN concentration over the plain regions of Northern India. This provides confidence that our configuration can be used for qualitative study of aerosol-urban-rainfall association at high resolution at a much lower computational cost than using the comprehensive WRF-Chem model.

2.4. Storm Events and Metrics Used for Analysis Over Various Cities

As mentioned earlier, the cities in Domain 3 experienced many mesoscale propagating (and raining) storms during our study period in the simulation. In general, these storms crossed a typical city within 2–4 h depending on the propagation speed and area of urban core of that city. First, hourly simulated rainfall data are used to identify and segregate the 2–3 h duration storm propagating events over major urban agglomerates (having more than five consecutive grids of urban LULC) in Domain 3. Analysis is performed over the cities in which more than 15 such propagating storm events were found. These cities include Delhi, Agra, Kanpur, Durgapur-Asansol agglomerate, and Kolkata located in the GB region. We have also performed analysis over Daman, Surat, Ahmedabad, Nagpur, Indore, and Varodara located in the western part of North India to compare and contrast between cities located within and outside the heavily polluted GB region. The locations of these cities are shown in Figure 1c.

While crossing the cities the storms produced nonuniform rainfall at the downwind, urban, and upwind regions of a city. We compare the rainfall over the urban core (as well as at the downwind region) of a city to its upwind region. Eighteen propagating storms were simulated over Kanpur. For each of storm event, we consider three equal-area boxes (equal to the area of the urban core of Kanpur) along the direction of the propagation of the storm across the city as shown in Figure 4. The total rainfall occurring within the box enclosing the urban core of a city during a propagating storm event is considered as urban rainfall. Similarly, the total rainfall occurring within the downwind box during the last hour of the storm event and the same over the upwind box during the first hour of the propagating storm event are referred as downwind rainfall and upwind rainfall, respectively, for that event. For storm events lasting for 2 h, the total rainfall over the urban box during both hours is considered, while urban rainfall occurring during the middle hour is only considered in case of a 3 h event. Similarly, urban, downwind, and upwind rainfall amounts for all the 18 storm events are calculated over Kanpur. Further, rainfall enhancement in urban region ($EnhRain_{urban}$, calculated as the difference between urban rainfall and upwind rainfall divided by the upwind rainfall) and downwind region ($EnhRain_{downwind}$, calculated as the difference between downwind and upwind rainfall divided by the upwind rainfall) with respect to the upwind region for each of the 18 storm events is calculated over Kanpur. It should be noted that the direction of storm propagation varied a lot among different cities as well as among different storms over the same city. For ease of calculation, we consider eight major directions of propagation (corresponding to storm entering from eight half-quarters of a circle). In addition, we consider that a storm entering an urban location from one of these eight directions can exit in three possible ways (Figure 4). Thus, the analysis accounts for 24 different possible storm propagation directions.

Mean CCN values near cloud base (900 hPa) within the urban box during the first hour of a particular storm is also recorded as the aerosol loading condition corresponding to that particular storm event. Later, the 18

Table 1
Details About the Land Use Land Cover Type Used and CCN Concentration Prescribed Over the Greater Kanpur Region for the Three Sensitivity Experiments

Experiment	LULC	CCN
CNTEX	URBAN over Kanpur city	Prescribed climatology
NOURBEX	Cropland over Kanpur city	Same as CNTEX
lowCCNEX	Same as CNTEX	Prescribed climatology in CNTEX/100

Note. LULC = land use land cover; CCN = cloud condensation nuclei; CNTEX = control experiment.

storm events are segregated into three equal bins resembling low (5–35 percentile of mean CCN values), middle (35–65 percentile of mean CCN values), and high (65–95 percentile of mean CCN values) CCN scenarios. The same methodology was used to create a CCNwise-sorted data set of $EnhRain_{downwind}$ and $EnhRain_{urban}$ from propagating storms over each of the remaining 10 identified cities. We ignore storms that partially crossed the urban regions, that is, storms that entered and exited through the adjacent sides of the urban box. Also, we only consider storms that produced rainfall over all the three regions of a city, that is, urban core, upwind, and downwind regions. These constrains are applied to ensure urban signature on rainfall distribution in our analysis.

2.5. Numerical Experiments Focused on a Case Study Over Kanpur

In this study, three additional 1 day simulations (5 August 2011) were performed (Table 1) to examine the relative role of LULC and CCN concentration on $EnhRain_{downwind}$ and $EnhRain_{urban}$ during a typical 3-hourly storm propagation event on 5 August 2011 over the greater Kanpur region. The storm propagated across the urban region of Kanpur in the northwest direction. In the control experiment (CNTEX), the domain structure and model configuration is kept similar to our default 15 day simulation with prescribed CCN climatology (Figure 1b) and default LULC pattern as obtained from MODIS data set. The Kanpur urban region is defined between 80.2°E–80.45°E and 26.4°N–26.55°E and surrounded by croplands on all sides. First, the spatiotemporal characteristics of the storm propagation and rainfall distribution around the urban region are studied. Further, for the second simulation (NOURBEX), the grids representing Kanpur city in the model (red color grids in Figure 1c) are replaced with cropland LULC to remove the effect of urban city on the simulated heavy rainfall event. As all the other factors remain the same, comparison of NOURBEX with CNTEX will illustrate the physical forcing (if any) of urban LULC on the rainfall distribution over the city center and downwind regions. Similarly, keeping all other things the same, the default CCN concentration over the greater Kanpur (grids within the area bounded by 80°E–80.7°E and 20.2°N–20.7°N in all the three domains) is reduced by a factor of 100 to resemble very clean conditions (~100 #/cm^3) in the third simulation (lowCCNEX). The role of CCN particles on the spatial distribution of rainfall will be investigated by comparing CNTEX and lowCCNEX runs. We used NCEP-FNL data available at a resolution of 1° × 1° for every 6 h to initialize all the experiments.

3. Results and Discussion

3.1. Observational Climatology Over Kanpur

Rainfall measurements from in situ rain gauges located at three different sites within the greater Kanpur including one at the city center (DBS), one at a rural site south of Kanpur city (JNV), and one at a semiurban location (IITK) north of Kanpur city are compared in Figure 5a. Computed hourly rain rate at each site is segregated into four intensity bins; 0.1–0.4 mm/h, 0.4–1 mm/h, 1–4 mm/h, and >4 mm/h, and the frequency distribution for each site is plotted (Figure 5b). These four bins represent <40, 40–70, 70–95, and >95 percentiles of the measured rainfall samples at IITK site, respectively. The lowest bin denotes drizzle conditions, and the highest bin represents extreme rainfall events. The number of rain events in the higher rainfall bins (>1 mm) at DBS station is more than 2 times of that over the JNV station. In contrast, the enhancement of rain events in the lower rainfall bins (<0.4 mm) at DBS station over JNV station is ~50%. Thus, the differences in rainfall between urban and rural site is mainly contributed from the heavy rainfall events.

The diurnal variation in frequency of hourly rainfall events is also compared at the three sites (Figure 5c). Most of the rainfall events over DBS occur between 1600 and 2000 LT, while the maximum rainfall occurrence over the JNV site is in the afternoon between 1400 and1700 LT. Like DBS, most of the rainfall in IITK also occurs during late evening between 1700 and 2000 LT. As UHI effect at Kanpur is stronger in late evening (Chakraborty et al., 2016) and can cause enhanced convection, the temporal differences in the fraction of rainfall occurrence between urban and rural sites indicate that UHI-induced convection effect might play a role in the spatial distribution of rainfall over the greater Kanpur. Comparison of bimonthly total rainfall over each site illustrates that the total rainfall over DBS is higher by ~50 mm in peak summer monsoon period (July–August) than IITK, followed by that at JNV (not shown). This is mainly because the frequency of rainfall events at DBS is higher for all the four intensity bins. Thus, in a climatological sense, this analysis illustrates

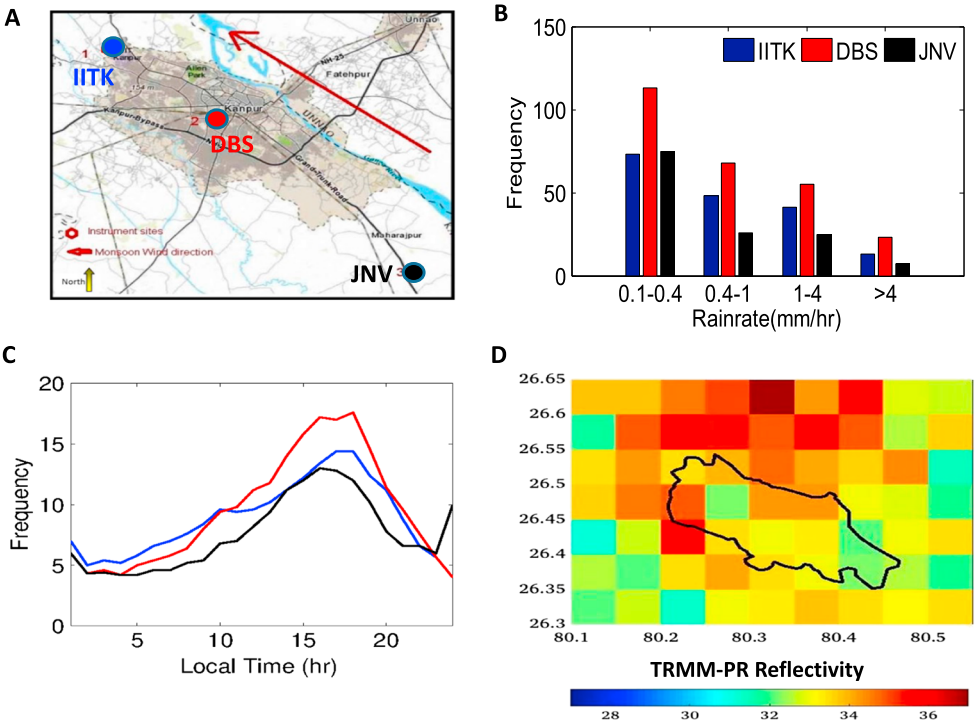

Figure 5. (a) The location of three automatic weather station stations in greater Kanpur. (b) Frequency of rainfall events in different rainfall intensity bins at the three sites. (c) Diurnal distribution of hourly rainfall occurrence frequency at the three sites. (d) Climatological mean spatial distribution of Tropical Rainfall Measuring Mission (TRMM)-PR observed radar reflectivity values at 2 km probable rainfall events (reflectivity >30 dBZ) over Greater Kanpur region.

that urban regions of the greater Kanpur receive more rainfall compared to nearby rural regions upwind of Kanpur. Previous studies have also reported changes in frequency, intensity, and duration of rainfall over cities in urban core (Bornstein & Lin, 2000; Changnon Jr et al., 1976, 1971; T.-C. Chen et al., 2007; Dou et al., 2015; Jauregui & Romales, 1996; Lei et al., 2008; Molders & Olson, 2004; Stout, 1969; J. Wang et al., 2012).

However, many studies also emphasized enhancement in downwind rainfall due to urban effect (Diem, 2008; Diem & Brown, 2003; Guo et al., 2006; Hand & Shepherd, 2009; Holt et al., 2006; Mote et al., 2007; Shem & Shepherd, 2009; Zhang et al., 2009, 2014). Huff and Changnon Jr (1972) identified increase in summer convective precipitation on the downwind side of urban regions using long-term data from St. Louis, Missouri, and other U.S. urban areas. But we did not find higher rainfall over the downwind site (IITK) of Kanpur compared to the urban site (DBS). This observation does not necessarily mean that rainfall over downwind region is lower than that at Kanpur core region, mainly because IITK might not be a representative downwind site of peak urban-induced rainfall modification. Recent studies have illustrated that the urban-induced effect on rainfall are manifested 30–80 km downwind of the cities in Unites States and India (Niyogi et al., 2017; Kishtawal et al., 2010). Therefore, we also have also used the TRMM-PR data set to create climatological mean spatial distribution of rainfall events around the greater Kanpur and check for modification in downwind rainfall. We used monsoon period for our data analysis during which the climatological wind direction at 850 hPa in reanalysis data sets is from southeast to northwest (not shown). Moreover, most of the (about 50–60%) summer monsoonal rainfall over northern India occurs under cyclonic monsoon depressions (Yoon & Chen, 2005), which generally form in the Bay of Bengal and propagate across the Indian landmass in a westward or northwestward direction (Krishnamurti & Bhalme, 1976; Riehl, 1971; Sikka, 1977). Thus, the northern and southern regions of Kanpur are usually downwind and upwind of Kanpur, respectively, during monsoonal rainfall events. The Z_e climatology clearly shows higher radar reflectivity (thus higher surface rainfall values) over the rural regions to the north of Kanpur city compared to the city core and southern rural regions (shown in Figure 5d), indicating that rainfall over downwind regions increases (even more than the urban regions) during high rainfall cases. Note that TRMM measurements are of coarse temporal resolution and

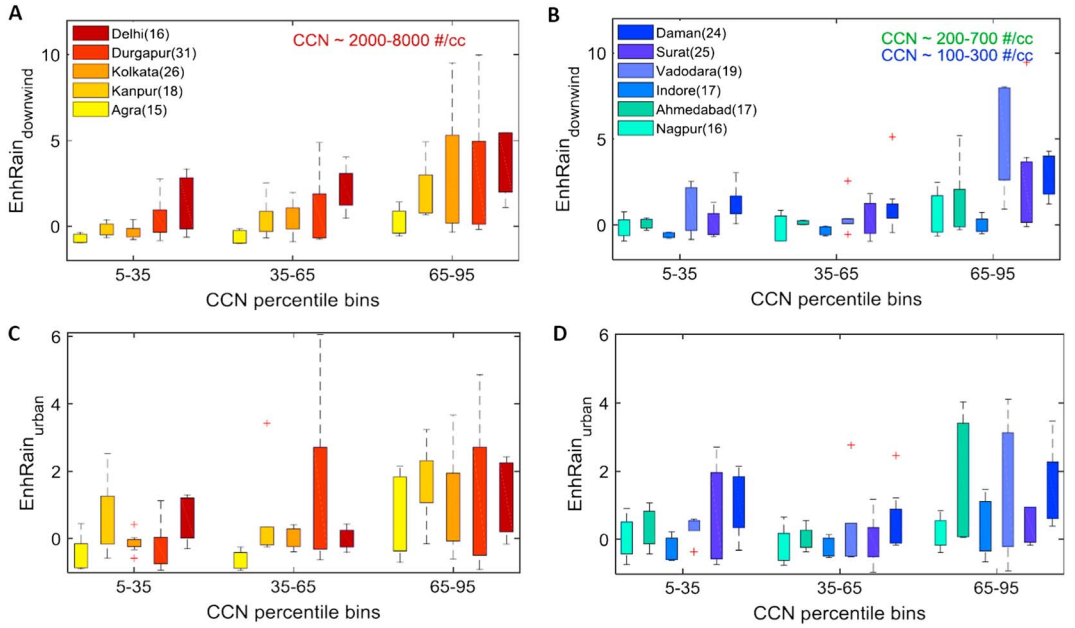

Figure 6. Top row shows boxplot distribution of Weather Research and Forecasting-simulated $EnhRain_{downwind}$ during propagating storms over different cities in (a) Gangetic Basin (warm color shades) and (b) non-Gangetic Basin region (cold color shades) of North India under low (5–35 percentile), middle (35–65 percentile), and high (65–95 percentile) cloud condensation nuclei (CCN) loading scenario. The location of the cities discussed here is marked in Figure 1c. The number (mentioned in brackets) after each city name in the legend is the number of simulated storms events over that city. The CCN concentration shown by different text colors in the legend denotes the simulated CCN range over cities in the corresponding group. Bottom row shows similar distribution for WRF-simulated $EnhRain_{urban}$ over cities in (c) Gangetic Basin and (d) non-Gangetic Basin region of North India. Please see methodology section for details on computation of $EnhRain_{downwind}$ and $EnhRain_{urban}$. The cities within each CCN bin are arranged in ascending order of the magnitude of their longitudinal (east-west) extend; that is, within each CCN bin, darker shade means longer east-west span of cities.

may not have captured the rainfall distribution during all propagating storms across Kanpur. However, use of 17 years of 3-hourly data set should present an accurate representation of the spatial pattern in rainfall over the region. Similar results were also found by Shepherd et al. (2002) around Atlanta, Georgia, using TRMM satellite-borne radar observations. Hence, both observations and simulations indicate the presence of local-scale urban-induced changes in rainfall distribution over the Greater Kanpur. However, it is not clear if the urban-rainfall association observed over Kanpur is a common phenomenon over the entire region. We next examine various simulated storm cases over 11 major cities in North India to answer the above question.

3.2. Relative Influence of LULC and CCN Concentration Over Rainfall

The variation in values of the WRF-simulated $EnhRain_{downwind}$ and $EnhRain_{urban}$ in the low, middle, and high CCN loading bins over different cities in Domain 3 (including Kanpur) is illustrated in Figure 6. The warm color shades (yellow and red) are used to mark the cities present within the GB region, while the cold color shades (green and blue) represent cities outside the GB region. This distinction is maintained here because the GB-based cities are more highly polluted (~2,000–8,000 #/cm^3 near cloud base) than the non-GB cities. Further, the green colored cities are relatively more polluted (~200–700 #/cm^3 near cloud base) than the blue colored cities (~100–300 #/cm^3 near cloud base). At the same time, the cities are also arranged from left to right within each CCN bin in an ascending order of their longitudinal extent (east-west span). This is done to visualize the effect of increasing urban area on $EnhRain_{downwind}$ and $EnhRain_{urban}$ within the narrow variability in CCN values. Here we used the longitudinal extent of an urban region as a proxy of the cross section of urbanized area encountered by a propagating storm because broadly we found that most of the simulated storms moved in the south-north direction (southeast to northwest and from southwest to northeast) in Domain 3 during our study period. Using the total area of urban cities does not introduce much variation to our analysis.

It is instantly clear that the $EnhRain_{downwind}$ and $EnhRain_{urban}$ values are largely positive (except in the low CCN bin) over all the cities located in the GB region (Figures 6a and 6c) suggesting enhancement in downwind and urban rainfall during storm propagation. But in most of the cities, the enhancement over downwind region is greater compared to that over urban region ($EnhRain_{downwind} > EnhRain_{urban}$). Interestingly, this phenomenon is also simulated in cities outside the GB region (Figures 6b and 6d).

Further, within each CCN bin, rainfall enhancement over downwind regions ($EnhRain_{downwind}$) increases as we move from left to right indicating a clear influence of urban LULC on $EnhRain_{downwind}$ and $EnhRain_{urban}$ from propagating storms over northern India. For instance, $EnhRain_{downwind}$ values are highest for Delhi (biggest among the analyzed cities in the GB) in each CCN bin (Figure 6a). Moreover, the distribution of $EnhRain_{urban}$ over Delhi also (Figure 6c) comprises greater values among the GB cities under similar CCN loading. Similar trend is also seen over Ahmedabad (Figures 6b and 6d; biggest among the green shaded cities) and Daman (Figures 6b and 6d; biggest among the blue shaded cities in non-GB region).

A comparison across CCN bins illustrates an increase in $EnhRain_{downwind}$ with increases in CCN loading for all the GB and non-GB cities (Figures 6a and 6b). Specifically, the distribution of $EnhRain_{downwind}$ is shifted toward higher values by a factor of 0.5–2 with an increase in CCN from low to high scenarios for both GB cities (Figure 6a) and non-GB cities (Figure 6b). However, the shift of $EnhRain_{downwind}$ across the CCN bins toward higher values in distribution is greater for the cities located in the GB compared to those located in the non-GB region. An increase in $EnhRain_{urban}$ with increases in CCN loading is also evident for GB and non-GB cities (Figures 6c and 6d), but the magnitude of shift of $EnhRain_{urban}$ is smaller than that of $EnhRain_{downwind}$ over all the analyzed cities irrespective of their locations in Domain 3. This suggests that $EnhRain_{downwind}$ is more closely associated with the CCN loading than the increase in $EnhRain_{urban}$ with CCN during storm passage over the cities.

In addition, the increase in $EnhRain_{downwind}$ values with increases in CCN loading is relatively larger (~2 times) over bigger cities (like Delhi and Kolkata) compared to that over smaller cities (Kanpur and Agra) in the GB region. Similar trends in $EnhRain_{downwind}$ are also observed for bigger non-GB cities (Daman and Surat) verses Indore (relatively smaller urban area). However, the change in $EnhRain_{urban}$ with increase in CCN loading is negligible over big cities like Surat, Daman, and Delhi, suggesting saturation of CCN effect on $EnhRain_{urban}$ over big cities located in both GB and non-GB regions. On the other extreme, the mean value of $EnhRain_{downwind}$ is negative and lower than that of $EnhRain_{urban}$ in the low CCN bin for cities having relatively small longitudinal extent (like Agra and Indore). These points together indicate an increase in downwind shift in rainfall occurrence with increase in both urban area and ambient CCN loading during propagating storms.

Thus, occurrence of higher amount of rainfall over urban and downwind region compared to upwind region is prevalent over many cities in North India irrespective of their locations. This phenomenon is in agreement with our observational analysis over Kanpur. Moreover, the relative influence of both the extent of urban region traversed as well as the ambient CCN loading on the distribution of rainfall from a propagating storm over urban and downwind region of the city is evident. Next, to gain a process level understanding of this phenomenon, we compare and discuss the results from our CCN and LULC 1 day numerical experiments.

3.3. Numerical Case Study: Simulation of a Typical Heavy Rainfall Event

Here we discuss the Domain 3 simulated weather over the greater Kanpur region (80°E–80.7°E and 26.2°N–26.7°N) between 1030 and 1330 LT, 5 August 2011. The hourly storm propagation is shown in Figure 7. The grids between 80.2°E–80.45°E and 26.4°N–26.55°N represent the urban Kanpur region (see Figure 7c). During 1030–1130 LT, rainfall occurred over many grids within the greater Kanpur region but the maxima are located near the south of the Kanpur urban region (Figure 7a). In the following hour, the location of the rainfall maxima is shifted northwestward to the urban center. Also, the regions to the north of Kanpur city received heavy rainfall during 1130–1230 LT (Figure 7b). The northwest storm propagation continued in 1230–1330 LT and the storm passed the city of Kanpur (Figure 7c).

In accordance with our previous methodology (Figure 4) two regions equal in area to the urban region, one each to the upwind and downwind of the urban region (bounded black boxes in Figure 7), are identified along the line of storm propagation across the city. The surface rainfall accumulated within these regions is averaged along the longitude and plotted on the rainfall-latitude plot for each hour separately and also

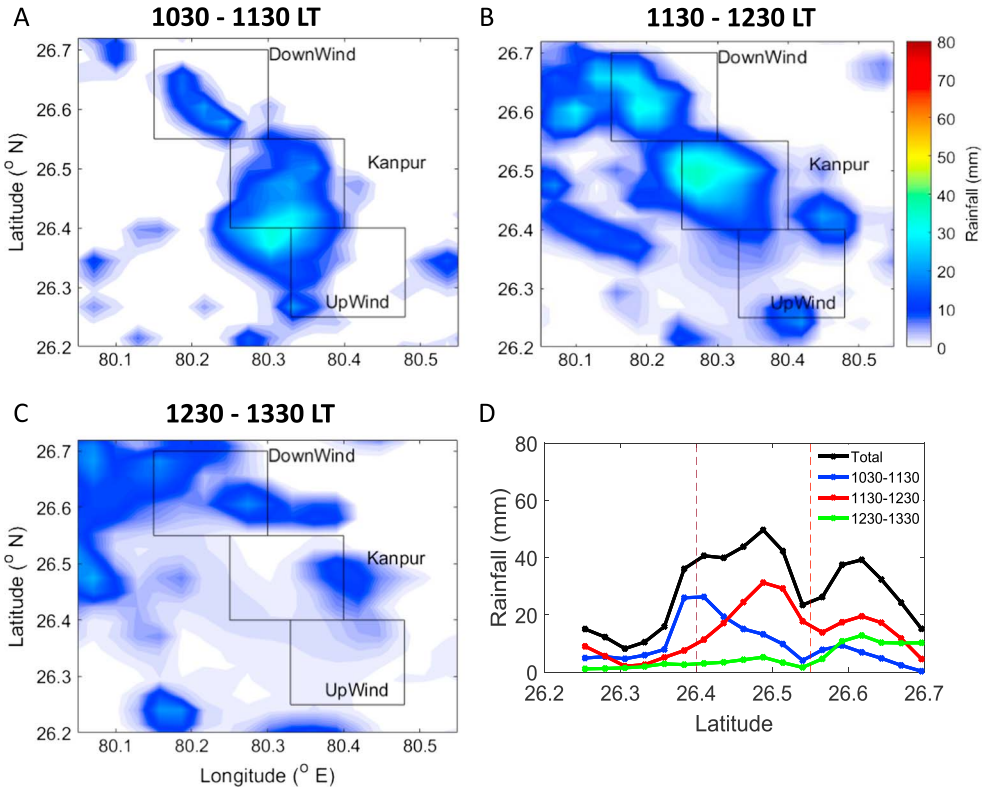

Figure 7. Spatial distribution of accumulated rainfall simulated over greater Kanpur region during (a) 10301130 LT, (b) 1130–1230 LT, and (c) 1230–1330 LT period. Three equal-area regions one each at the south, urban city center, and north of Kanpur city parallel to the line of storm propagation are shown in black boxes. (d) The surface rainfall longitudinally averaged over the grids present within the three bounded boxes plotted on a latitude-magnitude axis.

for the total rainfall during the 3 h combined (Figure 7d). The peak of rainfall (~20 mm) during the first hour coincided with the juxtaposition of the rural and urban regions at the upwind of the city, while the peak rainfall during the second and third hours occurred over the city center (~40 mm) and over the rural area ~10 km downwind of the city (~15 mm), respectively. Another interesting observation is that the rainfall amount increased linearly as the storm approached the city from the south, indicating the influence of the rural-urban juxtaposition on rainfall. Although, a spike in rainfall amount ~10 km downwind of the city is found, the spatial distribution of total rainfall during this event (1030–1330 LT) illustrates that the urban Kanpur region received almost double the amount of rainfall received by the adjoining rural areas. This is in agreement with our climatological spatial distribution of rainfall observed by TRMM-PR data and in situ measurements and thus can be considered as a typical rainfall event over this region.

3.3.1. CNTEX Versus NOURBEX

Replacing the urban LULC with cropland LULC in the NOURBEX simulations caused significant reduction in the accumulated surface rainfall (1030–1330 LT) over the Kanpur city compared to the CNTEX simulation (Figures 8a and 8b). Maximum reduction in rainfall is ~40 mm at city center. The total rainfall over the downwind box is also reduced, but there is negligible change in the surface rainfall over the upwind box. The spatial distribution illustrates that comparatively more rainfall occurred at the west side of the downwind region in the NOURBEX simulation (Figure 8b).

To understand the physical mechanism of the simulated differences in rainfall spatial distribution due only to a change in LULC type from urban to cropland over the central Kanpur region, the difference (CNTEX-NOURBEX) in surface temperature at 2 m and the surface energy fluxes during 0930–1030 LT is investigated. Figure 8c illustrates that the surface temperature at the center of Kanpur is reduced by a change in LULC from urban to cropland by ~0.3–0.5°C. A change in LULC type also affected the partitioning of available net radiation at the surface. Figures 8d–8f illustrate that the ground heat fluxes and sensible heat fluxes (SHF) are

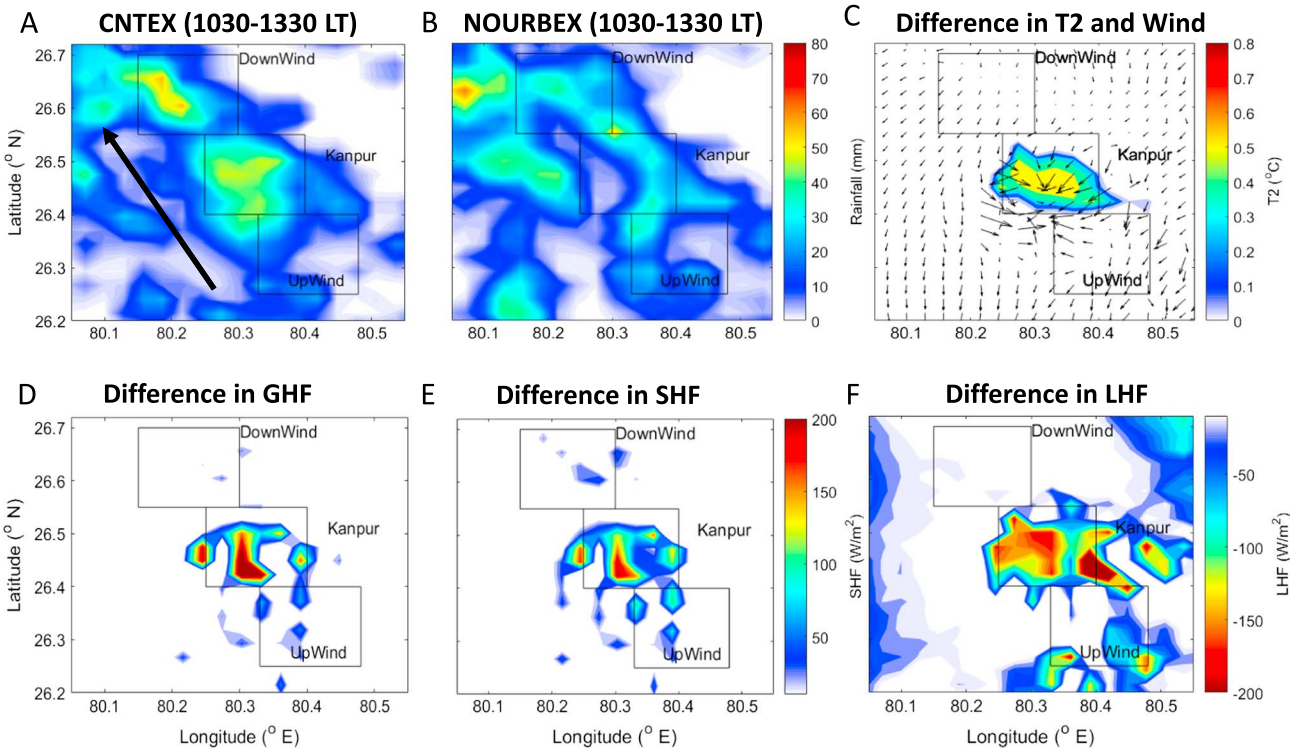

Figure 8. Spatial distribution of accumulated rainfall (1030–1330 LT) over greater Kanpur region during (a) CNTEX and (b) NOURBEX. The spatial distribution of differences (CNTEX-NOURBEX) in (c) temperature at 2 m and wind circulation at 950 hPa, (d) ground heat fluxes, (e) sensible heat fluxes, and (f) latent heat fluxes. The direction storm propagation is shown by the black arrow in Panel a. Three equal-area regions one each at the upwind, urban city center, and downwind of Kanpur city parallel to the line of storm propagation are shown in black boxes.

higher, but the latent heat fluxes (LHFs) are lower at the center of Kanpur region in the CNTEX simulations (urban LULC) compared to NOURBEX (natural LULC). Higher ground heat flux under urbanization causes more storage of available energy at the surface and increases the soil temperature. At the same time reduction in vegetation and availability of natural surface under urbanization causes reduction in evapotranspiration and reduces the LHF. This increases the soil-air temperature gradient, which, coupled with reduction in evapotranspiration, results in favorable dissipation of available energy via SHF, thereby enhancing the SHF under urbanization. The increase in SHF affects the near-surface layer and increases its temperature under urbanization, which causes UHI effect.

A similar anomaly (CNTEX-NOURBEX) in horizontal wind circulation at 950 hPa shows that under urban LULC the winds converge toward the urban core of Kanpur city (Figure 8c). Cross-sectional view of the differences in water vapor mixing ratio, vertical velocity, and cloud droplet water content profiles longitudinally averaged over *all the latitude grids within the three boxes* is plotted in Figure 9. Below 700 hPa altitude, higher moisture content (0.1 g/m^3) and higher temperature (not shown) are simulated over the city box in CNTEX. For CNTEX, the vertical velocity (W) is comparatively higher mainly above 800 hPa. Higher liquid water content in cloud droplets (maximum = 0.6 g/m^3 at ~800 hPa) is also simulated in the CNTEX runs. However, no significant change in ice hydrometeor content is observed from the change in the LULC type.

The following chain of feedbacks can explain these simulated differences between CNTEX and NOURBEX. The additional temperature available in near-surface atmospheric layers in CNTEX causes a low-pressure zone (not shown) that induces convergence of horizontal winds toward the city center. The higher prescribed surface roughness for the urban LULC also contributes to creation of this convergence zone. Enhanced influx of winds in CNTEX from all sides increases the moisture availability by overcompensating for the reduction in LHF. This convergence also induces enhanced updrafts which generate more cloud droplets and water mass content near cloud base and eventually occurrence of more rainfall over the Kanpur region and its downwind region (i.e., the northern box). Similar urban-land-convection-rainfall interactions are also seen over various other cities in previous modeling studies (Bornstein & Lin, 2000; Hand & Shepherd, 2009; Molders & Olson,

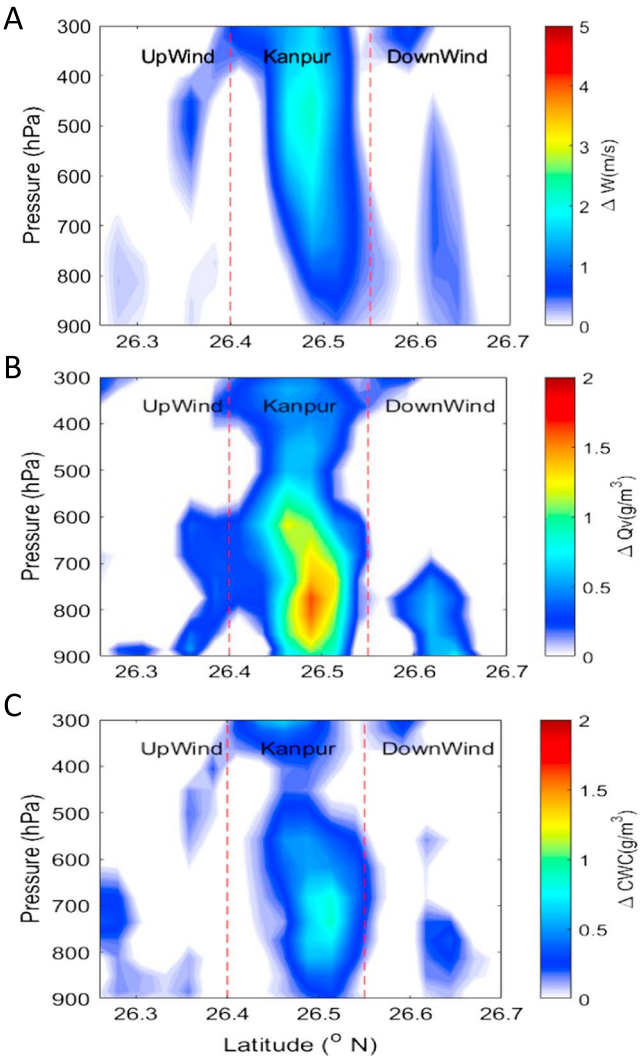

Figure 9. Latitude-altitude plot of differences (CNTEX-NOURBEX) in (a) vertical velocity (W), (b) water vapor mixing ratio (Q_v), and (c) cloud water content (CWC) profiles longitudinally averaged over the grids present within the three bounded boxes during 1130 LT.

2004; Shepherd et al., 2002). A lack of urban LULC resulted in lower convergence, reduced convection, and hence lower generation of cloud liquid and ice phase mass concentration over central Kanpur region, which resulted in downpour of higher amount of rainfall at a later stage when the storm propagated farther downwind of Kanpur. Thus, urban LULC can cause physical feedback to stimulate local cloud growth over cities and generate more rainfall from propagating storms.

3.4. CNTEX Versus lowCCNEX

The spatial distributions of accumulated surface rainfall (1030–1330 LT) from the CNTEX and lowCCNEX runs are illustrated in Figures 10a and 10b, respectively. For quantitative analysis, the fractional change in rainfall (CNTEX-lowCCNEX)/lowCCNEX with increase in CCN is averaged within the representative boxes along the longitude and plotted on a latitude-rainfall plot (Figure 10c). The vertical lines in Figure 10c illustrate the boundaries of the Kanpur urban box. For lowCCNEX, the storm is also centered over the upwind box during the first hour of our study and subsequently propagated toward the Kanpur urban center and downwind box in the second and third hour of our study (similar to as seen in Figure 7d), respectively.

Comparison of CNTEX and lowCCNEX clearly illustrates that under the high CCN scenario the accumulated surface rainfall amount (1030–1330 LT) is comparatively lower over many grids within the upwind box and over some grids within the urban box (Figures 10a and 10b). However, the accumulated rainfall amount is significantly higher over the downwind box under high CCN scenario. Quantitatively, Figure 10c shows that rainfall decreased by ~40% in the upwind box but increased by 10% and ~60% over the Kanpur urban box and the downwind box, respectively, with increases in CCN. This indicates that while more rainfall occurred during the 1030–1130 LT period in lowCCNEX, most of the downpour from the storm occurred during 1130–1330 LT in the CNTEX run. Moreover, the total accumulated rainfall over our study regions is higher in CNTEX compared to lowCCNEX run. This analysis indicates that the simulated differences in spatial distribution of rainfall between CNTEX and lowCCNEX are mainly due to CCN-induced temporal changes in rainfall occurrence during the storm propagation.

To better understand the spatiotemporal changes in rainfall, analysis of the spatiotemporal differences in cloud microphysical properties and vertical velocity (W; m/s) is performed. Figures 11a and 11b illustrate that the time- and longitude-averaged columnar sum of effective radius (Re) of cloud droplets is lower (by ~20–40%), but the number of cloud droplets is higher (by 2–4 times) under high CCN simulation except for a few grids in the downwind box. This is in accordance to the first aerosol indirect effect (Twomey, 1977). Further, time- and longitude-averaged columnar sum of liquid-phase mass concentration (i.e., a combination of cloud water content (CWC) and rainwater content (RWC)) and ice phase mass concentration (snow water content (SWC) + ice water content (IWC) + graupel water content (GWC)) is analyzed. Figures 11c and 11d show spatiotemporal changes similar to the differences found in rainfall (Figure 10c). The liquid and ice mass generated in clouds during the 1030–1130 LT period (initial part of the storm) is higher in lowCCNEX and the same is higher during 1130–1330 LT (later part of storm) in the CNTEX run. CWC + RWC increased by ~100% and IWC + SWC + GWC increased by ~50% over the region downwind of Kanpur during CNTEX compared to lowCCNEX.

A cross-sectional latitude-altitude view of mean differences in CWC, IWC + GWC + SWC, RWC, and W at each vertical layer during 1230–1330 LT is also plotted in Figures 12a–12d, respectively. Figure 12a illustrates that enhancement in cloud droplets is mainly located in the higher altitudes (above freezing level, i.e., ~500 hPa)

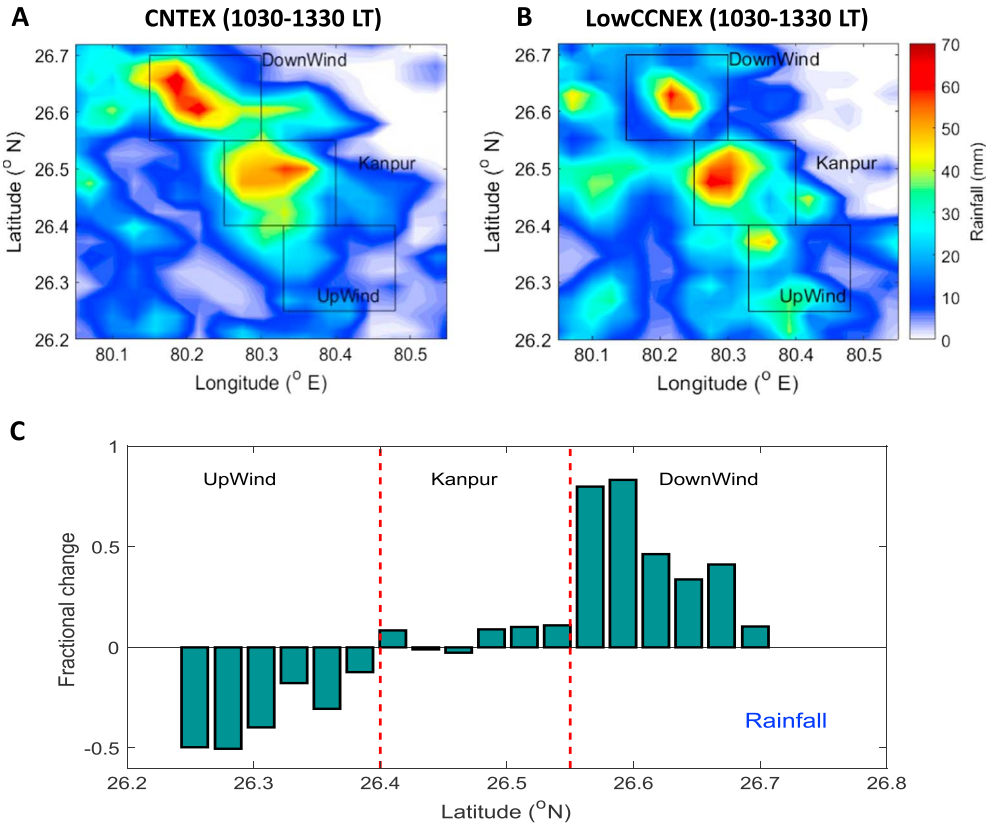

Figure 10. Spatial distribution of accumulated rainfall (1030–1330 LT) over greater Kanpur region during (a) control experiment (CNTEX) and (b) lowCCNEX. (c) The fractional change in rainfall with increase in CCN (CNTEX-lowCCNEX)/lowCCNEX is longitudinally averaged over all the latitude grids within the three boxes from 1030 to 1330 LT and plotted on a latitude-rainfall axis. Kanpur urban region lies within the vertical lines.

in the downwind box. Simultaneously, the mass of ice phase hydrometeors are also significantly enhanced at higher altitudes in the CNTEX run compared to the lowCCNEX run (Figure 12b). We found that increase in graupel particles is highest among the ice phase species. The enhanced cloud and ice phase hydrometeors are also associated with increase in RWC (Figure 12c) in the downwind region resulting in the increase in rainfall at surface. Considerable increase in vertical velocity (W) is also found above the freezing level over the downwind box between CNTEX and lowCCNEX (Figure 12d). The increase in updraft values is most probably associated with formation of higher amount of graupel hydrometeors due to rimming process between ice/snow particles and supercooled cloud droplets (Sarangi et al., 2015). These results are consistent with the CCN-induced cloud invigoration theory. Note that we found no significant differences in the temporal evolution of W during 1030–1230 LT with updraft being relatively very strong over the urban box (not shown). Moreover, it can be seen that during lowCCNEX, W was maximized over the urban box but for CNTEX the same was maximized over the downwind box after the storm crossed the urban Kanpur region.

The following feedback mechanisms can explain the above CCN-associated differences. Increase in CCN concentration is associated with formation of more cloud droplets with smaller effective radius, which leads to less efficient collision-coalescence process and delays raindrop formation (Rosenfeld, 1999; Squires, 1958). Concurrently, more condensation and smaller droplets also result in lower effective terminal velocity and higher cloud droplet mobility upward (Heiblum et al., 2016; Koren et al., 2015). In CNTEX, the CCN-induced enhanced buoyancy would push the smaller condensates above the freezing level (Andreae et al., 2004; Lensky & Rosenfeld, 2006) which, in turn, would enhance the presence of water mass as supercooled liquid above the freezing level. This process, in principle, releases more latent heat of freezing at higher altitudes and further invigorates the cloud system (Altaratz et al., 2014; Tao et al., 2012). Invigoration leads to further

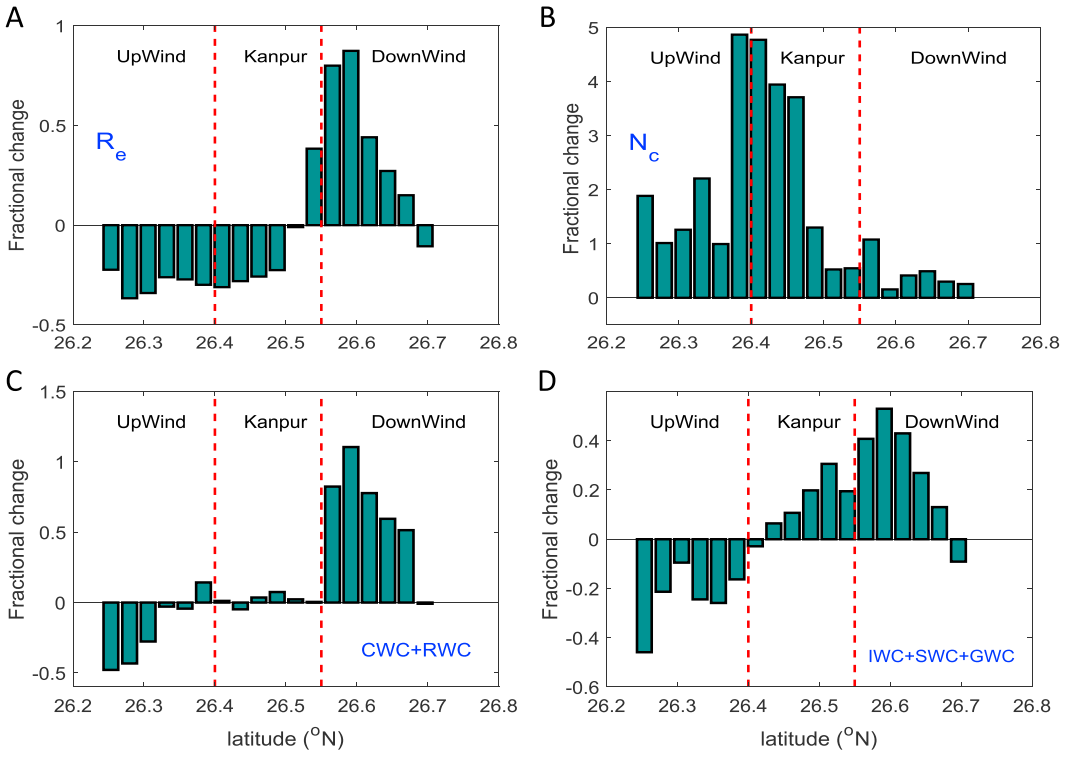

Figure 11. The fractional change (CNTEX-lowCCNEX)/lowCCNEX with increase in cloud condensation nuclei (CCN) in time- and longitude-averaged columnar sum of (a) Effective Radius (R_e), (b) Cloud droplet number concentration (N_c), (c) total mass of Liquid drops (CWC; cloud water content) + (RWC; rainwater content), and (d) total mass of ice phase hydrometeors (ice water content + snow water content and graupel water content; IWC + SWC + GWC) longitudinally accumulated over all the grids within the three boxes shown in Figure 10 from 1030 to 1330 LT. The fractional changes are plotted on a *y* axis. Kanpur urban region lies within the vertical hashed lines.

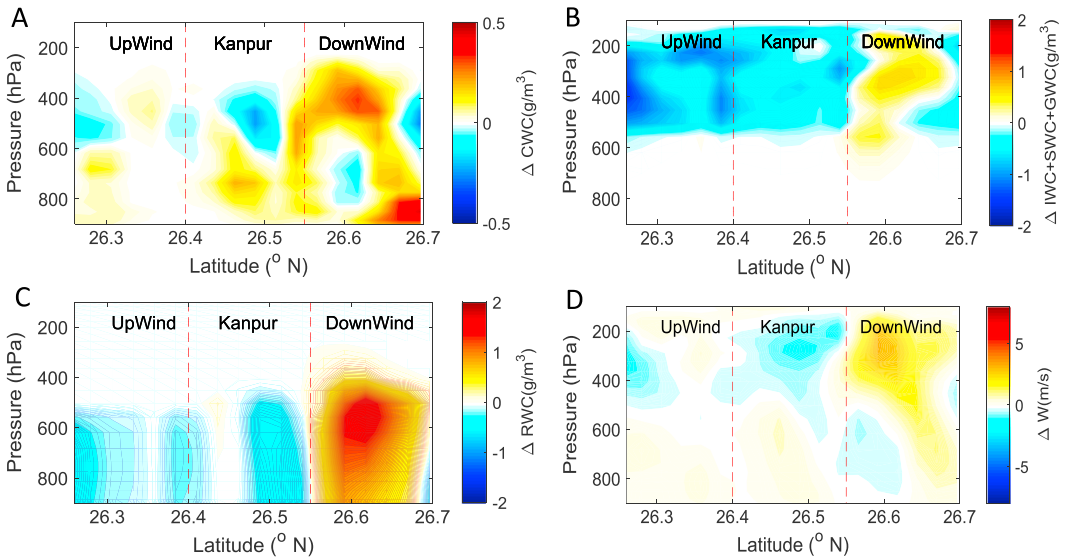

Figure 12. (a) Latitude-altitude plot of differences (CNTEX-lowCCN) in (a) cloud water content (CWC), (b) graupel water content (GWC; g/m^3) + snow water content (SWC; g/m^3) + ice water content (IWC; g/m^3), (c) rainwater content (RWC; g/m^3), and (d) vertical velocity (W; in units of m/s) longitudinally averaged over the grids present within the three bounded boxes during 1230–1330 LT.

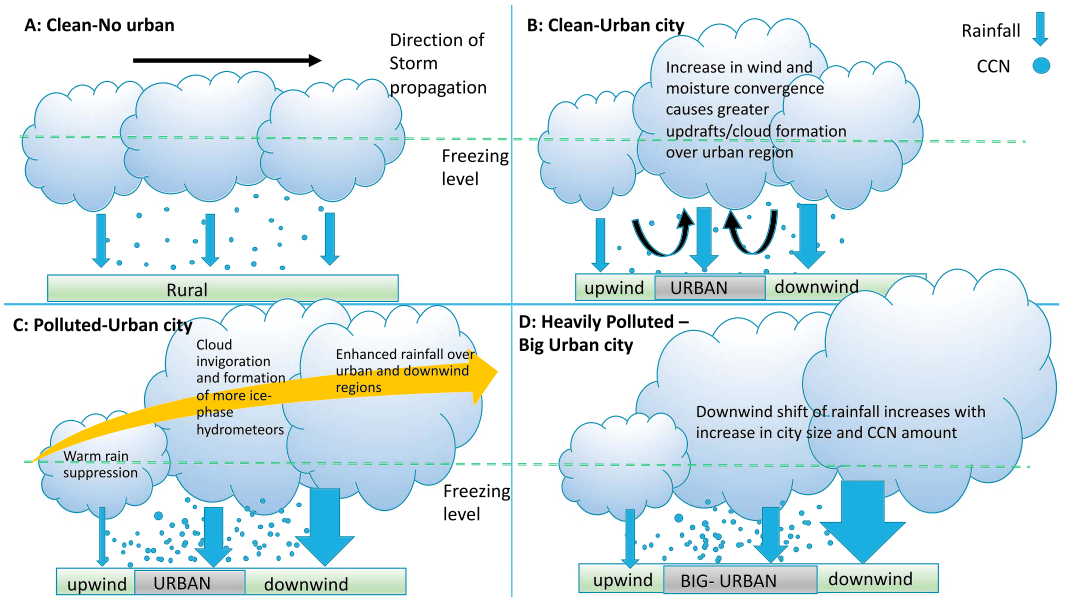

Figure 13. Schematic illustrations of the rainfall-cloud condensation nuclei (CCN)-urban land use land cover coupling and underlying processes found over (a) rural regions, (b) clean (low CCN) urban regions, (c) polluted urban regions, and (d) heavily polluted big urban centers in northern India.

enhancement in formation of ice phase hydrometeors at higher altitudes by freezing of small droplets (Altaratz et al., 2014) and increased ice-water accretion process (Ilotoviz et al., 2016; Sarangi et al., 2015), which eventually results in higher rain rate and surface rainfall (Andreae et al., 2004; Koren et al., 2005, 2012; Rosenfeld et al., 2008). Thus, on a temporal scale the feedbacks associated with CCN-induced cloud invigoration can be segregated into three stages. First, warm rainfall occurrence decreases under higher CCN concentration, followed by increase in water mass above freezing level and enhancement in mass concentration of ice phase hydrometers along with rainfall initiation in the next stage. Finally, the invigorated cloud system results in enhanced hydrometeor formation, which falls toward the surface, resulting in an increase in surface rainfall. Hence, rainfall increased in CNTEX after the storm crossed the Kanpur city as the enhanced number of hydrometeors eventually fall under gravity to the surface.

A combined view of these simulations illustrates that increase in frequency and magnitude of rainfall over the Kanpur urban core is mainly due to the urban land surface properties and associated changes in updraft values. However, increase in rainfall over downwind region of Kanpur during high-intensity rain cases is a combined result of urban LULC-induced high convective-convergence zone and CCN-induced changes in cloud microphysics. The high-intensity rainfall over this region occurs under propagating storms from south-east to northwest associated with organized mesoscale monsoon depressions. This cloud invigoration mechanism can also explain the variations in CCN-urban-rainfall associations between different cities as noted in the above section. With increase in urban area, not only the CCN surface emission increase but also the associated convective-convergence zone expands, resulting in more instability and updrafts. Therefore, the clouds associated with storms propagating across bigger cities are likely to get more invigorated with increase in CCN compared to that over relatively smaller cities. Enhancement in cloud invigoration will lead to greater spatiotemporal shift of rainfall occurrence toward downwind regions. Similar results are also reported in Schmid and Niyogi (2017) using idealized simulations. They showed that aerosol-induced micro-physical modifications initiate over urban city and persist downwind causing downwind shift of rainfall with increase in aerosols. Thus, with increase in CCN loading over bigger cities higher $EnhRain_{downwind}$ values were obtained, but $EnhRain_{urban}$ values remain the same or even decrease. To summarize, Figure 13 summarizes the effect of CCN and urban LULC on rainfall distribution under different possible scenarios using simple schematic diagrams. Logically, the presence of very high instability within the city and weak horizontal winds may result in intense, sudden, heavy downpour at the downwind part of the city and cause flash flooding.

4. Summary

The primary objective of this study is to investigate and understand the spatial distribution of rainfall around metropolitan cities located in central GB. We have used the greater Kanpur as a typical example mainly due to availability of in situ data from three AWS stations in and around Kanpur. Frequency-intensity analysis using 4 years (2013–2016) of data between June and September illustrates that the amount of surface rainfall received at the urban sites of Kanpur is significantly higher than regions located to the south of the city at hourly, daily, and bimonthly temporal resolutions. The frequency of rainfall occurrence in late evening is high over urban sites but not over the rural site. TRMM-PR observations at fine spatial resolution (5 km $\times$ 5 km) from 1998 to 2015 illustrate that downwind regions of greater Kanpur are prone to receive heavier rainfall compared to urban regions. Therefore, observational analysis clearly indicates the presence of urban signature on rainfall spatial distribution over the Greater Kanpur.

We used a high-resolution WRF simulation coupled with the Thompson aerosol-aware microphysics from 5 to 20 August 2011 (output at hourly frequency) to study rainfall enhancement over downwind and urban regions relative to the rainfall occurring in upwind regions during storm propagation across various cities in North India. Analysis of this data set supported that downwind enhancement of rainfall is a prevalent phenomenon not only over Kanpur but also over many other cities in North India irrespective of their location within or outside the GB region. Specifically, increase in urbanized area encountered by a storm and increase in ambient CCN concentration during the storm is associated with the amount of urban and downwind enhancement in rainfall.

Further, a representative heavy rainfall event that occurred on 5 August 2011 due to a northwestward propagating storm over the greater Kanpur is studied using three 1 day WRF simulations (as described in Table 1). First, the event is simulated with default configuration, but in the second experiment the grids representing urban LULC of Kanpur city in all the domains are replaced with cropland LULC. In the third experiment the default CCN concentration is reduced by a factor of 100 (only over the Greater Kanpur region) in all the domains to represent a clean scenario. The presence of urban LULC over Kanpur center increased the ground heat storage and SHF. This change in surface energy balance resulted in higher temperature in near-surface layer over urban regions. Increase in temperature led to formation of a low-pressure region and thereby convergence of winds at lower tropospheric heights over the city. This convergence resulted in enhanced updrafts and increase in cloud water mass concentration, which eventually led to an increase in surface rainfall over the urban region.

Comparison between high CCN and low CCN scenario simulations illustrated that aerosol microphysical effect can invigorate the clouds and perturb the spatiotemporal distribution of rainfall from the propagating storm. Increase in CCN concentration resulted in suppression of rainfall over the rural regions south of Kanpur and transport of more water mass above the freezing level. This caused cloud invigoration and formation of more ice phase hydrometeors which eventually increased the surface rainfall over the rural regions to the north of Kanpur. This explained the observation that the rural regions to the north (climatological upwind in monsoon) of the city received higher amount of rainfall than the regions lying south (climatological upwind in monsoon) of the city. Accordingly, enhancement in cloud invigoration over bigger cities compared to smaller cities (and thereby greater shift in rainfall occurrence toward the downwind regions even under similar CCN loading) will be expected as convection convergence increases with the urbanized area encountering propagating storms, as also seen in our analysis of simulated storms over various cities in North India.

This study puts forward robust evidence that the spatial distribution of rainfall over metropolitan cities in the North India can be resultant of a synergy of couplings between urban LULC and CCN-induced cloud invigoration effect. However, it should be noted that we have focused mainly on the qualitative associations rather than the quantitative estimates of the findings in this modeling work. Therefore, this study also put forward the necessity of more numerical and observational studies in future to illustrate robustness and gain quantitative understanding of this phenomenon (downwind shift of rainfall) over cities in India. Besides, in this study the direct effect of aerosols is not considered, which can affect the atmospheric thermodynamics and thereby cloud formation. Further, variations in the UHI-CCN-rainfall association due to their impact on storm morphology and intensity are also an interesting aspect to look into in future studies.

Acknowledgments
The authors gratefully acknowledge the financial support given by the Earth System Science Organization, Ministry of Earth Sciences, Government of India (grant: MM/NERC-MoES-03/2014/002) under INCOMPASS project. All data measurements over Kanpur are uploaded at http://www.weatherrisk.com. Authors also acknowledge funding from the Department of Science and Technology, India. The contributions of PNNL authors are supported by the U.S. Department of Energy's Office of Science as part of the Regional and Global Climate Modeling Program. The Pacific Northwest National Laboratory is operated for DOE by Battelle Memorial Institute under contract DE-AC05-76RL01830. We appreciate valuable suggestions by Dev Niyogi and two other reviewers. Lastly, insightful discussions with Mr Tirthankar Chakraborty is acknowledged.

References

Altaratz, O., Koren, I., Remer, L., & Hirsch, E. (2014). Review: Cloud invigoration by aerosols coupling between microphysics and dynamics. *Atmospheric Research*, *140-141*, 38–60. https://doi.org/10.1016/j.atmosres.2014.01.009

Andreae, M. O., Rosenfeld, D., Artaxo, P., Costa, A. A., Frank, G. P., Longo, K. M., & Silva-Dias, M. A. F. (2004). Smoking rain clouds over the Amazon. *Science*, *303*(5662), 1337–1342. https://doi.org/10.1126/science.1092779

Bhagat, R. B. (2011). *Emerging pattern of urbanisation in India* (Vol. 46, pp. 10–12). Mumbai, India: Economic and Political Weekly.

Bhat, G. S., & Kumar, S. (2015). Vertical structure of cumulonimbus towers and intense convective clouds over the South Asian region during the summer monsoon season. *Journal of Geophysical Research: Atmospheres*, *120*, 1710–1722. https://doi.org/10.1002/2014JD022552

Bhattu, D., & Tripathi, S. N. (2015). CCN closure study: Effects of aerosol chemical composition and mixing state. *Journal of Geophysical Research: Atmospheres*, *120*, 766–783. https://doi.org/10.1002/2014JD021978

Boos, W., Hurley, J., & Murthy, V. (2015). Adiabatic westward drift of Indian monsoon depressions. *Quarterly Journal of the Royal Meteorological Society*, *141*(689), 1035–1048. https://doi.org/10.1002/qj.2454

Bornstein, R., & Lin, Q. (2000). Urban heat islands and summertime convective thunderstorm in Atlanta: Three case studies. *Atmospheric Environment*, *34*(3), 507–516. https://doi.org/10.1016/S1352-2310(99)00374-X

Chakraborty, T., Sarangi, C., & Tripathi, S. N. (2016). Understanding diurnality and inter-seasonality of a sub-tropical urban heat island. *Boundary-Layer Meteorology*, *163*(2), 287–309. https://doi.org/10.1007/s10546-016-0223-0

Chang, H.-I., Niyogi, D., Kumar, A., Kishtawal, C., Dudhia, J., Chen, F., et al. (2009). Possible relation between land surface feedback and the post landfall structure of monsoon depressions. *Geophysical Research Letters*, *36*, L15826. https://doi.org/10.1029/2009GL037781

Changnon Jr, S. A., Huff, F. A., & Semonin, R. G. (1971). METROMEX: An investigation of inadvertent weather modification. *Bulletin of the American Meteorological Society*, *52*(10), 958–968. https://doi.org/10.1175/1520-0477(1971)052%3C0958:MAIOIW%3E2.0.CO;2

Changnon, S. A. Jr., Semonin, R. G., & Huff, F. A. (1976). A hypothesis for urban rainfall anomalies. *Journal of Applied Meteorology*, *15*(6), 544–560. https://doi.org/10.1175/15200450(1976)

Chen, F., & Dudhia, J. (2001). Coupling an advanced land surface–Hydrology model with the Penn State–NCAR MM5 modeling system. Part I: Model implementation and sensitivity. *Monthly Weather Review*, *129*(4), 569–585. https://doi.org/10.1175/1520-0493(2001)129%3C0569:CAALSH%3E2.0.CO;2

Chen, T.-C., Wang, S.-Y., & Yen, M.-C. (2007). Enhancement of afternoon thunderstorm activity by urbanization in a valley: Taipei. *Journal of Applied Meteorology and Climatology*, *46*(9), 1324–1340. https://doi.org/10.1175/JAM2526

Chin, M., Ginoux, P., Kinne, S., Torres, O., Holben, B. N., Duncan, B. N., et al. (2002). Tropospheric aerosol optical thickness from the GOCART model and comparisons with satellite and sun photometer measurements. *Journal of the Atmospheric Sciences*, *59*(3), 461–483. https://doi.org/10.1175/1520-0469(2002)059%3C0461:TAOTFT%3E2.0.CO;2

Clark, E., Bornstein, R., & Tam, Y. (1985). Current and potential anthropogenic moisture effects on the New York City planetary boundary layer. *Journal of the Air Pollution Control Association*, *35*(8), 831–835. https://doi.org/10.1080/00022470.1985.10465963

Colarco, P., da Silva, A., Chin, M., & Diehl, T. (2010). Online simulations of global aerosol distributions in the NASA GEOS-4 model and comparisons to satellite and ground-based aerosol optical depth. *Journal of Geophysical Research*, *115*, D14207. https://doi.org/10.1029/2009JD012820

Collier, C. (2006). The impact of urban areas on weather. *Quarterly Journal of the Royal Meteorological Society*, *132*(614), 1–25. https://doi.org/10.1256/qj.05.199

DeMott, P. J., Prenni, A. J., Liu, X., Kreidenweis, S. M., Petters, M. D., Twohy, C. H., et al. (2010). Predicting global atmospheric ice nuclei distributions and their impacts on climate. *Proceedings of the National Academy of Sciences of the United States of America*, *107*(25), 11,217–11,222. https://doi.org/10.1073/pnas.0910818107

Dey, S., & Di Girolamo, L. (2011). A decade of change in aerosol properties over the Indian subcontinent. *Geophysical Research Letters*, *38*, L14811. https://doi.org/10.1029/2011GL048153

Diem, J. E. (2008). Detecting summer rainfall enhancement within metropolitan Atlanta, Georgia USA. *International Journal of Climatology*, *28*(1), 129–133. https://doi.org/10.1002/joc.1560

Diem, J. E., & Brown, D. P. (2003). Anthropogenic impacts on summer precipitation in Central Arizona, U.S.A. *The Professional Geographer*, *55*(3), 343–355. https://doi.org/10.1111/00330124.5503011

Dou, J., Wang, Y., Bornstein, R., & Miao, S. (2015). Observed spatial characteristics of Beijing urban climate impacts on summer thunderstorms. *Journal of Applied Meteorology and Climatology*, *54*(1), 94–105. https://doi.org/10.1175/JAMC-D-13-0355.1

Dumka, U., Bhattu, D., Tripathi, S., Kaskaoutis, D., & Madhavan, B. (2015). Seasonal inhomogeneity in cloud precursors over Gangetic Himalayan region during GVAX campaign. *Atmospheric Research*, *155*, 158–175. https://doi.org/10.1016/j.atmosres.2014.11.022

Fan, J., Yuan, T., Comstock, J. M., Ghan, S., Khain, A., Leung, L. R., et al. (2009). Dominant role by vertical wind shear in regulating aerosol effects on deep convective clouds. *Journal of Geophysical Research*, *114*, D22206. https://doi.org/10.1029/2009JD012352

Ginoux, P., Chin, M., Tegen, I., Prospero, J. M., Holben, B., Dubovik, O., & Lin, S.-J. (2001). Sources and distributions of dust aerosols simulated with the GOCART model. *Journal of Geophysical Research*, *106*(D17), 20,255–20,273. https://doi.org/10.1029/2000JD000053

Givati, A., & Rosenfeld, D. (2004). Quantifying precipitation suppression due to air pollution. *Journal of Applied Meteorology*, *43*(7), 1038–1056. https://doi.org/10.1175/15200450(2004)043%C2%A11038:QPSDTA%C2%BF2.0.CO;2

Grell, G. A., & Freitas, S. R. (2014). A scale and aerosol aware stochastic convective parameterization for weather and air quality modeling. *Atmospheric Chemistry and Physics*, *14*(10), 5233–5250. https://doi.org/10.5194/acp-14-5233-2014

Guo, X., Fu, D., & Wang, J. (2006). Mesoscale convective precipitation system modified by urbanization in Beijing City. *Atmospheric Research*, *82*(1-2), 112–126. https://doi.org/10.1016/j.atmosres

Gupta, A. K., & Nair, S. S. (2011). Urban floods in Bangalore and Chennai: Risk management challenges and lessons for sustainable urban ecology. *Current Science*, *100*(11), 1638–1645. Retrieved from www.jstor.org/stable/24077767

Hand, L. M., & Shepherd, J. M. (2009). An investigation of warm-season spatial rainfall variability in Oklahoma City: Possible linkages to urbanization and prevailing wind. *Journal of Applied Meteorology and Climatology*, *48*(2), 251–269. https://doi.org/10.1175/2008JAMC2036.1

Hazra, A., Goswami, B. N., & Chen, J.-P. (2013). Role of interactions between aerosol radiative effect, dynamics, and cloud microphysics on transitions of monsoon intraseasonal oscillations. *Journal of the Atmospheric Sciences*, *70*(7), 2073–2087. https://doi.org/10.1175/JASD-12-0179.1

Hazra, A., Chaudhari, H. S., Ranalkar, M., & Chen, J.-P. (2017). Role of interactions between cloud microphysics, dynamics and aerosol in the heavy rainfall event of June 2013 over Uttarakhand, India. *Quarterly Journal of the Royal Meteorological Society*, *143*(703), 986–998. https://doi.org/10.1002/qj.2983

Heiblum, R. H., Altaratz, O., Koren, I., Feingold, G., Kostinski, A. B., Khain, A. P., et al. (2016). Characterization of cumulus cloud fields using trajectories in the center of gravity versus water mass phase space: 2. Aerosol effects on warm convective clouds. *Journal of Geophysical Research: Atmospheres*, *121*, 6356–6373. https://doi.org/10.1002/2015JD024193

Holt, T. R., Niyogi, D., Chen, F., Manning, K., LeMone, M. A., & Qureshi, A. (2006). Effect of land–atmosphere interactions on the IHOP 24–25 May 2002 convection case. *Monthly Weather Review*, *134*(1), 113–133. https://doi.org/10.1175/MWR3057.1

Huff, F., & Changnon Jr, S. (1972). Climatological assessment of urban effects on precipitation at St. Louis. *Journal of Applied Meteorology*, *11*(5), 823–842. https://doi.org/10.1175/1520-0450(1972)011%3C0823:CAOUEO%3E2.0.CO;2

Iguchi, T., Meneghini, R., Awaka, J., Kozu, T., & Okamoto, K. (2000). Rain profiling algorithm for TRMM precipitation radar data. *Advances in Space Research*, *25*(5), 973–976. https://doi.org/10.1016/S0273-1177(99)00933-3, remote Sensing and Applications: Earth, Atmosphere and Oceans

Ilotoviz, E., Khain, A. P., Benmoshe, N., Phillips, V. T. J., & Ryzhkov, A. V. (2016). Effect of aerosols on freezing drops, hail, and precipitation in a mid-latitude storm. *Journal of the Atmospheric Sciences*, *73*(1), 109–144. https://doi.org/10.1175/JAS-D-14-0155.1

Janjic, Z. (2002). Nonsingular implementation of the Mellor-Yamada level 2.5 scheme in the NCEP Meso model.

Jauregui, E., & Romales, E. (1996). Urban effects on convective precipitation in Mexico City. *Atmospheric Environment*, *30*(20), 3383–3389. https://doi.org/10.1016/1352-2310(96)00041-6

Jin, M., & Shepherd, J. M. (2005). Inclusion of urban landscape in a climate model: How can satellite data help? *Bulletin of the American Meteorological Society*, *86*(5), 681–690. https://doi.org/10.1175/BAMS-86-5-681

Kaufmann, R. K., Seto, K. C., Schneider, A., Liu, Z., Zhou, L., & Wang, W. (2007). Climate response to rapid urban growth: Evidence of a human-induced precipitation deficit. *Journal of Climate*, *20*(10), 2299–2306. https://doi.org/10.1175/JCLI4109.1

Khain, A., & Lynn, B. (2009). Simulation of a supercell storm in clean and dirty atmosphere using weather research and forecast model with spectral bin microphysics. *Journal of Geophysical Research*, *114*, D19209. https://doi.org/10.1029/2009JD011827

Khain, A. P., Benmoshe, N., & Pokrovsky, A. (2008). Factors determining the impact of aerosols on surface precipitation from clouds: An attempt at classification. *Journal of Atmospheric Science*, *65*(6), 1721–1748. https://doi.org/10.1175/2007JAS2515.1

Kishtawal, C. M., Niyogi, D., Tewari, M., Pielke, R. A., & Shepherd, J. M. (2010). Urbanization signature in the observed heavy rainfall climatology over India. *International Journal of Climatology*, *30*(13), 1908–1916. https://doi.org/10.1002/joc.2044

Koop, T., Luo, B., Tsias, A., & Peter, T. (2000). Water activity as the determinant for homogeneous ice nucleation in aqueous solutions. *Nature*, *406*(6796), 611–614. https://doi.org/10.1038/35020537

Koren, I., Kaufman, Y. J., Rosenfeld, D., Remer, L. A., & Rudich, Y. (2005). Aerosol invigoration and restructuring of Atlantic convective clouds. *Geophysical Research Letters*, *32*, L14828. https://doi.org/10.1029/2005GL023187

Koren, I., Altaratz, O., Remer, L. A., Feingold, G., Martins, J. V., & Heiblum, R. H. (2012). Aerosol-induced intensification of rain from the tropics to the mid-latitudes. *Nature Geoscience*, *5*(2), 118–122. https://doi.org/10.1038/ngeo1364

Koren, I., Altaratz, O., & Dagan, G. (2015). Aerosol effect on the mobility of cloud droplets. *Environmental Research Letters*, *10*(10), 104011. https://doi.org/10.1088/1748-9326/10/10/104011

Krishnamurti, T. N., & Bhalme, H. N. (1976). Oscillations of a monsoon system. Part I. Observational aspects. *Journal of Atmospheric Science*, *33*(10), 1937–1954. https://doi.org/10.1175/1520-0469(1976)033%3C1937:OOAMSP%3E2.0.CO;2

Kummerow, C., Barnes, W., Kozu, T., Shiue, J., & Simpson, J. (1998). The tropical rainfall measuring mission (TRMM) sensor package. *Journal of Atmospheric and Oceanic Technology*, *15*(3), 809–817. https://doi.org/10.1175/1520-0426(1998)015%3C0809:TTRMMT%3E2.0.CO;2

Kummerow, C., Simpson, J., Thiele, O., Barnes, W., Chang, A. T. C., Stocker, E., et al. (2000). The status of the tropical rainfall measuring mission (TRMM) after two years in orbit. *Journal of Applied Meteorology*, *39*(12), 1965–1982. https://doi.org/10.1175/1520-0450(2001)040%3C1965:TSOTTR%3E2.0.CO;2

Lei, M., Niyogi, D., Kishtawal, C., Pielke Sr, R. A., Beltrn-Przekurat, A., Nobis, T., & Vaidya, S. (2008). Effect of explicit urban land surface representation on the simulation of the 26 July 2005 heavy rain event over Mumbai, India. *Atmospheric Chemistry and Physics*, *8*(20), 5975–5995. https://doi.org/10.5194/acp-8-5975-2008

Lensky, I. M., & Rosenfeld, D. (2006). The time-space exchangeability of satellite retrieved relations between cloud top temperature and particle effective radius. *Atmospheric Chemistry and Physics*, *6*(10), 2887–2894. https://doi.org/10.5194/acp-6-2887-2006

Levin, Z., & Cotton, W. (2008). *Aerosol pollution impact on precipitation: A scientific review*. Berlin: Springer.

Li, W., & Schumacher, C. (2011). Thick anvils as viewed by the TRMM precipitation radar. *Journal of Climate*, *24*(6), 1718–1735. https://doi.org/10.1175/2010JCLI3793.1

Li, W., Chen, S., Chen, G., Sha, W., Luo, C., Feng, Y., et al. (2011). Urbanization signatures in strong versus weak precipitation over the pearl river delta metropolitan regions of China. *Environmental Research Letters*, *6*(3), 034020. https://doi.org/10.1088/1748-9326/6/3/034020

Li, Z., Lau, W., V Ramanathan, G. X. W., Ding, Y., Manoj, M., Liu, J., et al. (2016). Aerosol and monsoon climate interactions over Asia. *Reviews of Geophysics*, *54*(4), 866–929. https://doi.org/10.1002/2015RG000500

Lowry, W. P. (1977). Empirical estimation of urban effects on climate: A problem analysis. *Journal of Applied Meteorology*, *16*(2), 129–135. https://doi.org/10.1175/1520-0450(1977)016%3C0129:EEOUEO%3E2.0.CO;2

Misra, A., Kanawade, V. P., & Nand Tripathi, S. (2016). Quantitative assessment of AOD from 17 CMIP5 models based on satellite-derived AOD over India. *Annales Geophysicae*, *34*(8), 657–671. https://doi.org/10.5194/angeo-34-657-2016

Mitra, C., Shepherd, J. M., & Jordan, T. (2012). On the relationship between the premonsoonal rainfall climatology and urban land cover dynamics in Kolkata city, India. *International Journal of Climatology*, *32*(9), 1443–1454. https://doi.org/10.1002/joc.2366

Mlawer, E. J., Taubman, S. J., Brown, P. D., Iacono, M. J., & Clough, S. A. (1997). Radiative transfer for inhomogeneous atmospheres: RRTM, a validated correlated-k model for the longwave. *Journal of Geophysical Research*, *102*(D14), 16,663–16,682. https://doi.org/10.1029/97JD00237

Molders, N., & Olson, M. A. (2004). Impact of urban effects on precipitation in high latitudes. *Journal of Hydrometeorology*, *5*(3), 409–429. https://doi.org/10.1175/1525-7541(2004)005%3C0409:IOUEOP%3E2.0.CO;2

Mote, T. L., Lacke, M. C., & Shepherd, J. M. (2007). Radar signatures of the urban effect on precipitation distribution: A case study for Atlanta, Georgia. *Geophysical Research Letters*, *34*, L20710. https://doi.org/10.1029/2007GL031903

Niyogi, D., Pyle, P., Lei, M., Arya, S. P., Kishtawal, C. M., Shepherd, M., et al. (2011). Urban modification of thunderstorms: An observational storm climatology and model case study for the Indianapolis urban region*. *Journal of Applied Meteorology and Climatology*, *50*(5), 1129–1144. https://doi.org/10.1175/2010JAMC1836.1

Niyogi, D., Lei, M., Kishtawal, C., Schmid, P., & Shepherd, M. (2017). Urbanization impacts on the summer heavy rainfall climatology over the Eastern United States. *Earth Interactions*, *21*(5), 1–17. https://doi.org/10.1175/EI-D-15-0045.1

Ntelekos, A. A., Smith, J. A., Baeck, M. L., Krajewski, W. F., Miller, A. J., & Goska, R. (2008). Extreme hydro meteorological events and the urban environment: Dissecting the 7 July 2004 thunderstorm over the Baltimore MD Metropolitan Region. *Water Resources Research*, *44*(8), W08446. https://doi.org/10.1029/2007WR006346

Oke, T. R. (2002). *Boundary layer climates*. London: Routledge.
Orville, R. E., Huffines, G., Nielsen-Gammon, J., Zhang, R., Ely, B., Steiger, S., et al. (2001). Enhancement of cloud-to-ground lightning over Houston, Texas. *Geophysical Research Letters*, *28*(13), 2597–2600. https://doi.org/10.1029/2001GL012990
Phillips, V. T., DeMott, P. J., & Andronache, C. (2008). An empirical parameterization of heterogeneous ice nucleation for multiple chemical species of aerosol. *Journal of the Atmospheric Sciences*, *65*(9), 2757–2783. https://doi.org/10.1175/2007JAS2546.1
Pielke, R. A. (2001). Influence of the spatial distribution of vegetation and soils on the prediction of cumulus convective rainfall. *Reviews of Geophysics*, *39*(2), 151–177. https://doi.org/10.1029/1999RG000072
Pielke, R. A., Andy, P., Dev, N., Rezaul, M., Clive, M. A., Faisal, H., et al. (2011). Land use/land cover changes and climate: Modeling analysis and observational evidence. *WIREs Climate Change*, *2*(6), 828–850. https://doi.org/10.1002/wcc.144
Prabha, T. V., Patade, S., Pandithurai, G., Khain, A., Axisa, D., Pradeep-Kumar, P., et al. (2012). Spectral width of premonsoon and monsoon clouds over Indo-Gangetic valley. *Journal of Geophysical Research*, *117*, D20205. https://doi.org/10.1029/2011JD016837
Qian, Y., Gong, D., Fan, J., Leung, L. R., Bennartz, R., Chen, D., & Wang, W. (2009). Heavy pollution suppresses light rain in China: Observations and modeling. *Journal of Geophysical Research*, *114*, D00K02. https://doi.org/10.1029/2008JD011575
Riehl, H. (1971). A weather pattern. (Book reviews: Monsoon meteorology). *Science*, *172*, 691–692. https://doi.org/10.1126/science.172.3984.691
Rosenfeld, D. (1999). TRMM observed first direct evidence of smoke from forest fires inhibiting rainfall. *Geophysical Research Letters*, *26*(20), 3105–3108. https://doi.org/10.1029/1999GL006066
Rosenfeld, D. (2000). Suppression of rain and snow by urban and industrial air pollution. *Science*, *287*(5459), 1793–1796. https://doi.org/10.1126/science.287.5459.1793
Rosenfeld, D., & Woodley, W. (2003). Closing the 50-year circle: From cloud seeding to space and back to climate change through precipitation physics. In *Cloud Systems, Hurricanes, and the Tropical Rainfall Measuring Mission (TRMM), Meteorological Monographs* (Vol. 51, pp. 59–80).
Rosenfeld, D., Lohmann, U., Raga, G. B., O'Dowd, C. D., Kulmala, M., Fuzzi, S., et al. (2008). Flood or drought: How do aerosols affect precipitation? *Science*, *321*(5894), 1309–1313. https://doi.org/10.1126/science.1160606
Roy, A., Chatterjee, A., Sarkar, C., Das, S. K., Ghosh, S. K., & Raha, S. (2017). A study on aerosol-cloud condensation nuclei (CCN) activation over eastern Himalaya in India. *Atmospheric Research*, *189*, 69–81. https://doi.org/10.1016/j.atmosres.2017.01.015
Sarangi, C., Tripathi, S. N., Tripathi, S., & Barth, M. C. (2015). Aerosol-cloud associations over Gangetic Basin during a typical monsoon depression event using WRF-Chem simulation. *Journal of Geophysical Research: Atmospheres*, *120*, 10,974–10,995. https://doi.org/10.1002/2015JD023634
Sarangi, C., Tripathi, S. N., Kanawade, V. P., Koren, I., & Pai, D. S. (2017). Investigation of the aerosol–cloud–rainfall association over the Indian summer monsoon region. *Atmospheric Chemistry and Physics*, *17*(8), 5185–5204. https://doi.org/10.5194/acp-17-5185-2017
Schmid, P. E., & Niyogi, D. (2013). Impact of city size on precipitation-modifying potential. *Geophysical Research Letters*, *40*(19), 5263–5267. https://doi.org/10.1002/grl.50656
Schmid, P. E., & Niyogi, D. (2017). Modeling urban precipitation modification by spatially heterogeneous aerosols. *Journal of Applied Meteorology and Climatology*, *56*(8), 2141–2153. https://doi.org/10.1175/JAMC-D-16-0320.1
Seifert, A., Köhler, C., & Beheng, K. D. (2012). Aerosol-cloud-precipitation effects over Germany as simulated by a convective-scale numerical weather prediction model. *Atmospheric Chemistry and Physics*, *12*(2), 709–725. https://doi.org/10.5194/acp-12-709-2012
Shastri, H., Paul, S., Ghosh, S., & Karmakar, S. (2015). Impacts of urbanization on Indian summer monsoon rainfall extremes. *Journal of Geophysical Research: Atmospheres*, *120*, 496–516. https://doi.org/10.1002/2014JD022061
Shem, W., & Shepherd, M. (2009). On the impact of urbanization on summertime thunderstorms in Atlanta: Two numerical model case studies. *Atmospheric Research*, *92*(2), 172–189. https://doi.org/10.1016/j.atmosres.2008.09.013
Shepherd, J. M. (2005). A review of current investigations of urban-induced rainfall and recommendations for the future. *Earth Interactions*, *9*(12), 1–27. https://doi.org/10.1175/EI156.1
Shepherd, J. M., Pierce, H., & Negri, A. J. (2002). Rainfall modification by major urban areas: Observations from spaceborne rain radar on the TRMM satellite. *Journal of Applied Meteorology*, *41*(7), 689–701. https://doi.org/10.1175/1520-0450(2002)041%3C0689:RMBMUA%3E2.0.CO;2
Sikka, D. R. (1977). Some aspects of the life history, structure and movement of monsoon depressions. *Pure and Applied Geophysics*, *115*(5-6), 1501–1529. https://doi.org/10.1007/BF00874421
Simpson, M., Raman, S., Suresh, R., & Mohanty, U. (2008). Urban effects of Chennai on sea breeze induced convection and precipitation. *Journal of Earth System Science*, *117*(6), 897–909. https://doi.org/10.1007/s12040-008-0075-1
Singh, J., Vittal, H., Karmakar, S., Ghosh, S., & Niyogi, D. (2016). Urbanization causes nonstationarity in Indian summer monsoon rainfall extremes. *Geophysical Research Letters*, *43*(21), 11,269–11,277. https://doi.org/10.1002/2016GL071238
Squires, P. (1958). The microstructure and colloidal stability of warm clouds. *Tellus*, *10*(2), 256–261.
Srivastava, M., Tripathi, S., Dwivedi, A., Dalai, R., Bhattu, D., Bharti, P., et al. (2013). CCN closure results from Indian Continental Tropical Convergence Zone (CTCZ) aircraft experiment. *Atmospheric Research*, *132-133*, 322–331. https://doi.org/10.1016/j.atmosres.2013.05.025
Stout, G. E. (1969). Some observations of cloud initiation in industrial areas
Tao, W.-K., Chen, J.-P., Li, Z., Wang, C., & Zhang, C. (2012). Impact of aerosols on convective clouds and precipitation. *Reviews of Geophysics*, *50*, RG2001. https://doi.org/10.1029/2011RG000369
Teller, A., & Levin, Z. (2006). The effects of aerosols on precipitation and dimensions of subtropical clouds: A sensitivity study using a numerical cloud model. *Atmospheric Chemistry and Physics*, *6*(1), 67–80. https://doi.org/10.5194/acp-6-67-2006
Thompson, G., & Eidhammer, T. (2014). A study of aerosol impacts on clouds and precipitation development in a large winter cyclone. *Journal of the Atmospheric Sciences*, *71*(10), 3636–3658. https://doi.org/10.1175/JAS-D-13-0305.1
Thompson, G., Rasmussen, R. M., & Manning, K. (2004). Explicit forecasts of winter precipitation using an improved bulk microphysics scheme. Part I: Description and sensitivity analysis. *Monthly Weather Review*, *132*(2), 519–542. https://doi.org/10.1175/1520-0493(2004)132%3C0519:EFOWPU%3E2.0.CO;2
Thompson, G., Field, P. R., Rasmussen, R. M., & Hall, W. D. (2008). Explicit forecasts of winter precipitation using an improved bulk microphysics scheme. Part II: Implementation of a new snow parameterization. *Monthly Weather Review*, *136*(12), 5095–5115. https://doi.org/10.1175/2008MWR2387.1
Twomey, S. (1977). The influence of pollution on the shortwave albedo of clouds. *Journal of Atmospheric Science*, *34*(7), 1149–1152. https://doi.org/10.1175/1520-0469(1977)034%3C1149:TIOPOT%3E2.0.CO;2
Ulbrich, C. W., & Atlas, D. (1998). Rainfall Microphysics and Radar Properties: Analysis Methods for Drop Size Spectra. *Journal of Applied Meteorology*, *37*, 912–923.
Van den Heever, S. C., Carri'o, G. G., Cotton, W. R., Demott, P. J., & Prenni, A. J. (2006). Impacts of nucleating aerosol on Florida storms. Part I: Mesoscale simulations. *Journal of Atmospheric Science*, *63*(7), 1752–1775. https://doi.org/10.1175/JAS3713.1

Wang, H., Skamarock, W. C., & Feingold, G. (2009). Evaluation of scalar advection schemes in the advanced research WRF model using large-eddy simulations of aerosol-cloud interactions. *Monthly Weather Review*, *137*(8), 2547–2558. https://doi.org/10.1175/2009MWR2820.1

Wang, J., Zhang, R., & Wang, Y. (2012). Areal differences in diurnal variations in summer precipitation over Beijing metropolitan region. *Theoretical and Applied Climatology*, *110*(3), 395–408. https://doi.org/10.1007/s00704-012-0636-8

Yan, Z.-W., Wang, J., Xia, J.-J., & Feng, J.-M. (2016). Review of recent studies of the climatic effects of urbanization in China. *Advances in Climate Change Research*, *7*(3), 154–168. https://doi.org/10.1016/j.accre.2016.09.003, including special topic on atmospheric black carbon and its effects on cryosphere

Yang, B., Zhang, Y., & Qian, Y. (2012). Simulation of urban climate with high-resolution WRF model: A case study in Nanjing, China. *Asia-Pacific Journal of Atmospheric Sciences*, *48*(3), 227–241. https://doi.org/10.1007/s13143-012-0023

Yang, L., Tian, F., & Niyogi, D. (2015). A need to revisit hydrologic responses to urbanization by incorporating the feedback on spatial rainfall patterns. *Urban Climate*, *12*, 128–140. https://doi.org/10.1016/j.uclim.2015.03.001

Yang, X., Leung, L. Y., Zhao, N., Zhao, C., Qian, Y., Hu, K., et al. (2017). Contribution of urbanization to the increase of extreme heat events in an urban agglomeration in East China. *Geophysical Research Letters*, *44*(13), 6940–6950. https://doi.org/10.1002/2017GL074084

Yoon, J.-H., & Chen, T.-C. (2005). Water vapor budget of the Indian monsoon depression. *Tellus A*, *57*(5), 770–782. https://doi.org/10.1111/j.1600-0870.2005.00145.x

Zhang, C. L., Chen, F., Miao, S. G., Li, Q. C., Xia, X. A., & Xuan, C. Y. (2009). Impacts of urban expansion and future green planting on summer precipitation in the Beijing metropolitan area. *Journal of Geophysical Research*, *114*, D02116. https://doi.org/10.1029/2008JD010328

Zhang, Y., Smith, J. A., Luo, L., Wang, Z., & Baeck, M. L. (2014). Urbanization and rainfall variability in the Beijing metropolitan region. *Journal of Hydrometeorology*, *15*(6), 2219–2235. https://doi.org/10.1175/JHM-D-13-0180.1

Zhong, S., Qian, Y., Zhao, C., Leung, R., & Yang, X.-Q. (2015). A case study of urbanization impact on summer precipitation in the greater Beijing metropolitan area: Urban heat island versus aerosol effects. *Journal of Geophysical Research: Atmospheres*, *120*, 10,903–10,914. https://doi.org/10.1002/2015JD023753

Zhong, S., Qian, Y., Zhao, C., LY Leung, H. W., Yang, B., Fan, J., et al. (2017). Urbanization-induced urban heat island and aerosol effects on climate extremes in the Yangtze River Delta Region of China. *Atmospheric Chemistry and Physics*, *17*(8), 5439–5457. https://doi.org/10.5194/acp-17-5439-2017